J. Fluid Mech. (1996), *vol.* 306, *pp.* 223–265

Three-dimensional kinematic dynamos dominated by strong differential rotation

By GRAEME R. SARSON† AND DAVID GUBBINS

Department of Earth Sciences, University of Leeds, Leeds LS2 9JT, UK

(Received 1 June 1995 and in revised form 29 August 1995)

In the kinematic dynamo problem a fluid motion is specified arbitrarily and the induction equation is solved for non-decaying magnetic fields; it forms part of the larger magnetohydrodynamic (MHD) dynamo problem in which the fluid flow is buoyancy-driven. Although somewhat restrictive, the kinematic problem is important for two reasons: first, it suffers from numerical difficulties that are holding up progress on the MHD problem; secondly, for the geodynamo, it is capable of reproducing details of the observable magnetic field. It is more efficient to study these two aspects for the kinematic dynamo than for the full MHD dynamo. We explore solutions for a family of fluid flows in a sphere, first studied by Kumar & Roberts (1975), that is heuristically representative of convection in a rotating sphere such as the Earth's core. We guard against numerical difficulties by comparing our results with well-understood solutions from the axisymmetric ($\alpha\omega$) limit of Braginskiĭ (1964*a*) and with solutions of the adjoint problem, which must yield identical eigenvalues in an adequate numerical treatment. Previous work has found a range of steady dipolar solutions; here we extend these results and find solutions of other symmetries, notably oscillatory and quadrupolar fields. The surface magnetic fields, important for comparison with observations, have magnetic flux concentrated by downwelling flow. Roberts (1972) found that meridional circulation promoted stationary solutions of the $\alpha\omega$-equations, preferred solutions being oscillatory when no such circulation was present. We find analogous results for the full three-dimensional problem, but note that in the latter case the 'effective' meridional circulation arising from the non-axisymmetric convection (a concept made precise in the asymptotic limit of Braginskiĭ 1964*a*) must be considered. Thus stationary solutions are obtained even in the absence of 'true' meridional circulation, and the time-dependence can be controlled by the strength of the convection as well as by the meridional circulation. The preference for fields of dipole or quadrupole parity is largely controlled by the sign of the velocity: a reversal of velocity from a case favouring a dipole will favour quadrupole parity, and vice versa. For the comparison problem of Proctor (1977*b*) this symmetry is exact; for the physical problem the boundary conditions make a difference. The boundary effect is first removed by surrounding the dynamo region with a thick layer of quiescent conducting fluid, and then studied numerically by progressively reducing the thickness of this layer to zero. The insulating boundary contributes to the difficulty of obtaining dynamo action, and to the numerical difficulties encountered. The effect of an inner boundary on dynamo action is also considered, but found to be slight.

† Present address: Department of Mathematics, University of Exeter, Exeter EX4 4QE, UK.

1. Introduction

The Earth's magnetic field is generated by inductive action of fluid motion in the liquid iron core. The fluid flow is driven by buoyancy forces, probably associated with variations in composition of the liquid, and it regenerates magnetic field by doing work against the magnetic Lorentz force. This geodynamo process is similar to that acting to generate magnetic fields in the Sun and stars, except that much less energy is available to drive convection and the electric currents decay more rapidly because iron is a relatively poor conductor of electricity. In fact the geodynamo's energy budget is rather tight; thermodynamic arguments show the internal field cannot exceed a few tens of milliTeslas and must be restricted to large length scales (Gubbins, Masters & Jacobs 1979). This has two important benefits for modelling. First, electromagnetic shielding by the Earth's solid mantle and magnetized crust mean that short-wavelength features are in any case unobservable. Secondly, the accurate simulation of short-wavelength features would require a model of numerical resolution greater than is presently feasible.

The full dynamo problem is formidable and has therefore usually been studied in its constituent parts; a thorough review is given by Roberts & Gubbins (1987) and Roberts (1987). Much recent work has concentrated on the convection problem, either without magnetic field or with an imposed magnetic field, or on the simplified 'mean-field' $\alpha\omega$ dynamo problem (discussed below). In this paper we concentrate on the now relatively neglected kinematic dynamo problem, in which the fluid flow is prescribed and one searches for instabilities in the form of exponentially growing magnetic fields (dynamo instabilities). The problem is somewhat artificial because the flow is arbitrary and not governed by an equation of motion. Although it is linear in the magnetic field, and so mathematically straightforward, severe numerical difficulties have previously been encountered in its study; solutions adequately represented by the finite numerical resolutions attainable have proven difficult to obtain. These are probably the main reasons for its neglect. We present three separate reasons why its study is now critical:

(*a*) We can explore the dynamo action of fluid flows that resemble those generated by convection. This is much simpler than attempting to solve the full dynamo problem, and we can hope to gain insight into what features of convective flow are essential for efficient dynamo action before conducting a full nonlinear calculation.

(*b*) The numerical difficulties encountered appear to have been associated only with the induction equation, so that by isolating them in the kinematic problem we hope to gain insight into how to circumvent them.

(*c*) If we are to be guided by observation in explaining in the geodynamo, our model must be capable of producing a magnetic field to compare with that observed at the surface of the core. Only a three-dimensional (3D) model can do this, and the extensive 3D calculations required for such a scheme are only practical for the simpler kinematic problem.

In the current paper we address the first and second of these points; the use of kinematic calculations in understanding the observed geodynamo has been considered in Hutcheson & Gubbins (1994) and Gubbins & Sarson (1994).

The kinematic dynamo problem has enjoyed a long and rather undistinguished history. The first results were negative, with anti-dynamo theorems such as those of Cowling (see e.g. Hide & Palmer 1982), suggesting the whole concept of a homogeneous dynamo might be untenable. The first numerical calculations were over-ambitious and resulted in solutions that, although initially convincing, were later shown to

be numerical artefacts (Bullard & Gellman 1954; Lilley 1970). The first successful dynamos were highly artificial (Backus 1958; Herzenberg & Lowes 1957), but numerical problems were eventually overcome (G. O. Roberts, reported in Roberts 1971; Gubbins 1972, 1973; Pekeris, Accad & Shkoller 1973) and Kumar & Roberts (1975) demonstrated convincing numerical convergence of magnetic fields generated by flows with the qualitative features of rotating convection. In this paper we take their study further.

The flows of Kumar & Roberts (1975, referred to herein as KR) contained three ingredients: differential rotation, known to be present in the Sun and to be a common feature of convection in rotating systems; columnar convection, of the type normally associated with rapidly rotating convective systems, essential for dynamo action; and meridional circulation (purely axisymmetric overturning) which Roberts (1972) found promoted the production of stationary magnetic fields. As well as investigating the importance for dynamo action of each of these components, we introduce another parameter to allow variation in the nature of the boundary employed, since some earlier work has shown that an external region of stationary fluid can, under certain circumstances, facilitate dynamo action (Bullard & Gubbins 1977; Hutcheson & Gubbins 1994).

KR were guided by the earlier work of Braginskiĭ (1964*a*, *b*), who developed an asymptotic theory for flows dominated by differential rotation. The relevant points of this theory are reviewed in §2; it is particularly suited to the geodynamo, which is dominantly axially dipolar in form, because it leads to simple axisymmetric equations appropriate to a nearly axisymmetric magnetic field. The essential effects of the non-axisymmetric fluid flow and magnetic field appear asymptotically as an induced e.m.f. parallel to the axisymmetric part of the magnetic field, and an 'effective' meridional circulation. The first of these features is the well-known α-effect, found in the later work of Steenbeck, Krause & Rädler (1966) (see also Roberts & Stix 1971; Krause & Rädler 1980) on turbulent dynamos, which has been successfully applied to the solar dynamo; the second effect is specific to Braginsky's theory, and has been relatively neglected. The simplified α-effect equations have been the subject of many studies, both kinematic and dynamic. The most relevant study for this paper is that of Roberts (1972), who explored the link between meridional circulation and the time-dependence and spatial symmetry of the magnetic field solution.

We view the kinematic dynamo as a stability problem. The fluid flow is specified and the resulting linear induction equation solved for magnetic field solutions of exponential time-dependence. The flow is described by a small number of parameters, one of which is the magnetic Reynolds number, which we treat as our control parameter in our search for marginally stable solutions. We seek the instability boundary in this space of parameters by direct numerical calculation. This numerical approach is the only one available for a problem that contains the complicated elements of spherical geometry and departures from axial symmetry, but it has limitations. If we find a satisfactorily converged solution at marginal stability we may claim to have demonstrated dynamo action, but from negative results we may only claim the absence of dynamo action below some upper limit on the magnetic Reynolds number set by the numerical procedure.

The KR fluid flow is invariant under two important spatial operations, reflection in the equatorial plane and rotation by an angle π about the polar axis; these invariances lead to four possible symmetries of magnetic field solutions. Gubbins & Zhang (1993) show that decoupling of these symmetries occurs also in the full dynamo problem. We refer to that work for a full discussion, but discuss the symmetry properties relevant

to our specific investigation in §2.2. Previous work has concentrated on magnetic field solutions containing the axial dipole term because these are the most geophysically interesting, but the physically realizable solution is simply the most unstable; therefore in the following work we consider all possible solutions.

2. Formulation of the problem

2.1. *The kinematic dynamo problem of Kumar & Roberts*

The induction equation is non-dimensionalized with velocity and length scales $\mathscr{U}$, $\mathscr{L}$, and diffusion time $\mathscr{L}^2/\eta$, where η is the magnetic diffusivity, to give

$$\mathscr{D}\boldsymbol{B} = \frac{\partial \boldsymbol{B}}{\partial t} - R_m \nabla \times (\boldsymbol{u} \times \boldsymbol{B}) - \nabla^2 \boldsymbol{B} = 0, \tag{2.1a}$$

where $\boldsymbol{u}$ is the fluid velocity, $\boldsymbol{B}$ the magnetic field, and $R_m = \mathscr{U}\mathscr{L}/\eta$ is the magnetic Reynolds number. We consider only incompressible flows so that both $\boldsymbol{u}$ and $\boldsymbol{B}$ are solenoidal.

The value of $\boldsymbol{u}$ is prescribed, leaving (2.1a) linear in $\boldsymbol{B}$, and we seek solutions of the form $\boldsymbol{B}_0(r,\theta,\phi)\exp\lambda t$ with $\operatorname{Re}\lambda = 0$. (The subscript '0' will subsequently be dropped for convenience.) The corresponding value of R_m, if such a solution exists, is called the critical magnetic Reynolds number, R_m^c. The kinematic dynamo problem consists of finding R_m^c and the corresponding $\boldsymbol{B}$, and frequency $\omega = \operatorname{Im}\lambda$, for a chosen $\boldsymbol{u}$.

We consider a conducting sphere V, given by $r < 1$ in spherical coordinates (r,θ,ϕ), surrounded by an infinite insulating volume $\hat{V}$. The magnetic field in V, $\boldsymbol{B}(r,\theta,\phi)$, must satisfy (2.1$a$), whilst the field in the current-free region $\hat{V}$, $\hat{\boldsymbol{B}}(r,\theta,\phi)$, must satisfy

$$\nabla \times \hat{\boldsymbol{B}} = 0, \qquad r > 1, \tag{2.1b}$$

$$\hat{\boldsymbol{B}} = O(r^{-3}), \qquad r \to \infty. \tag{2.1c}$$

Continuity of $\boldsymbol{B}$ requires

$$\boldsymbol{B} = \hat{\boldsymbol{B}}, \qquad r = 1. \tag{2.1d}$$

Expanding $\boldsymbol{B}$ in toroidal and poloidal vector spherical harmonics,

$$\boldsymbol{B} = \boldsymbol{T} + \boldsymbol{S} = \nabla \times [T(r,\theta,\phi)\,\boldsymbol{e}_r] + \nabla \times \nabla \times [S(r,\theta,\phi)\,\boldsymbol{e}_r], \tag{2.2a}$$

$$T(r,\theta,\phi) = \sum_{l=1}^{\infty}\sum_{m=0}^{l} T_l^{mc}(r)P_l^m(\cos\theta)\cos m\phi + T_l^{ms}(r)P_l^m(\cos\theta)\sin m\phi, \tag{2.2b}$$

$$S(r,\theta,\phi) = \sum_{l=1}^{\infty}\sum_{m=0}^{l} S_l^{mc}(r)P_l^m(\cos\theta)\cos m\phi + S_l^{ms}(r)P_l^m(\cos\theta)\sin m\phi, \tag{2.2c}$$

where P_l^m are associated Legendre functions (see e.g. Abramowitz & Stegun 1965) and $\boldsymbol{e}_r$ the unit radial vector, allows the condition of continuity with the external potential field to be expressed via matching conditions on the toroidal and poloidal scalars,

$$T_l^m = 0, \qquad \frac{\mathrm{d}S_l^m}{\mathrm{d}r} + \frac{l}{r}S_l^m = 0, \qquad r = 1. \tag{2.3}$$

We also require regularity at the origin,

$$T_l^m = O(r^{l+1}), \qquad S_l^m = O(r^{l+1}), \qquad r \to 0, \tag{2.4}$$

a condition also imposed on the prescribed velocity.

We follow KR in investigating the class of flows defined by

$$\boldsymbol{u} = \epsilon_0 \boldsymbol{t}_1^0 + \epsilon_1 \boldsymbol{s}_2^0 + \epsilon_2 \boldsymbol{s}_2^{2c} + \epsilon_3 \boldsymbol{s}_2^{2s}, \tag{2.5}$$

where the ϵ_i are variable parameters and the $\boldsymbol{t}$, $\boldsymbol{s}$ are toroidal and poloidal vector spherical harmonics in the decomposition of $\boldsymbol{u}$,

$$\boldsymbol{u} = \boldsymbol{t} + \boldsymbol{s} = \nabla \times [t(r,\theta,\phi)\,\boldsymbol{e}_r] + \nabla \times \nabla \times [s(r,\theta,\phi)\,\boldsymbol{e}_r], \tag{2.6}$$

in terms of a spherical harmonic expansion analogous to that in (2.2*a*). The radial functions adopted by KR, defined for $0 \leqslant r \leqslant 1$, are

$$t_1^0(r) = r^2(1-r^2), \tag{2.7a}$$

$$s_2^0(r) = r^6(1-r^2)^3, \tag{2.7b}$$

$$s_2^{2s}(r) = r^4(1-r^2)^2 \cos(pr), \tag{2.7c}$$

$$s_2^{2c}(r) = r^4(1-r^2)^2 \sin(pr); \tag{2.7d}$$

p is here an integer multiple of π, and determines the radial complexity (number of cells) of the convective motion.

This flow represents a combination of differential rotation (t_1^0), axisymmetric meridional circulation (s_2^0), and non-azimuthally mirror-symmetric convection (s_2^2). These combine to allow dynamo action according to the Braginskiĭ (1964*a*) theory discussed in §2.4.

Apart from the detailed forms of radial function employed, this flow incorporates flows studied by other authors as special cases. The first study, by Bullard & Gellman (1954), had $\epsilon_1 = \epsilon_2 = 0$. Lilley (1970) considered flows with $\epsilon_1 = 0$, as did Hutcheson (1990) and Nakajima & Kono (1991). Dudley & James (1989) and Hutcheson & Gubbins (1994) have reported calculations based on the full KR flow. Axisymmetric flows obtained by setting $\epsilon_2 = \epsilon_3 = 0$ can also generate magnetic fields of quite different symmetry, for different radial functions (Dudley & James 1989).

2.2. *Symmetries of the solutions*

Symmetry properties of the full dynamo problem are discussed by Gubbins & Zhang (1993). Following their notation, we denote reflection in the equatorial plane, $\theta \to \pi - \theta$, by E, and rotation by an angle $2\pi/M$ about the polar axis, $\phi \to \phi + 2\pi/M$, by P_M. If these operations are accompanied by a change of sign, they are denoted by E^A and P_M^A respectively; if not, by E^S and P_M^S. (The superscript A denotes anti-symmetric, S, symmetric.) Symmetry of field is then defined via invariance under these operations.

The KR velocity can be seen to be invariant under both the E^S and P_2^S operations. This results in four separate symmetries of magnetic fields, each invariant under one of the possible combinations of E^A, E^S, P_2^A, P_2^S (see table 1). A full stability analysis must consider each of these solution types, as the physically realized mode will be the most unstable (that with smallest R_m^c); only $E^A P_2^S$ solutions have been reported to date. For the linear kinematic dynamo these solutions are independent and may be superimposed. The nonlinear MHD dynamo allows only the $E_S P_2^S$ and $E_A P_2^S$ solutions in isolation; the nonlinear terms couple the P_2^A solutions with the P_2^S.

A further symmetry of the velocity is invariance under translation in time, which admits periodic solutions; this is consistent, of course, with the exponential time-dependence required from the linear nature of the problem.

Further symmetries in the flow reduce the parameter space to be explored, as noted by Dudley & James (1989). Rotation by $\pi/2$ about the polar axis, $\phi \to \phi + \pi/2$, is equivalent to the mapping $(\epsilon_2 \to -\epsilon_2, \epsilon_3 \to -\epsilon_3)$; inversion in the plane $\phi = 0$,

E	P_2	Toroidal	Poloidal	m	Nomenclature
E^A	P_2^S	$l-m$ even	$l-m$ odd	m even	Axial dipole
E^A	P_2^A	$l-m$ even	$l-m$ odd	m odd	Equatorial quadrupole
E^S	P_2^S	$l-m$ odd	$l-m$ even	m even	Axial quadrupole
E^S	P_2^A	$l-m$ odd	$l-m$ even	m odd	Equatorial dipole

TABLE 1. Magnetic field symmetries of the four solutions, and their decomposition in spherical harmonics (degree l, order m), in an expansion of the magnetic field into toroidal and poloidal parts. The 'equatorial quadrupole' label is used rather loosely to denote the symmetry whose leading poloidal spherical harmonic term is $l = 2$, $m = 1$.

$\phi \to -\phi$, is equivalent to $(\epsilon_0 \to -\epsilon_0, \epsilon_2 \to -\epsilon_2)$. As the problem must be invariant under these operations, these two parameter mappings, plus their compound mapping and the identity mapping, form a group of four parameter mappings under which the solution is invariant:

$$(\epsilon_0, \epsilon_1, \epsilon_2, \epsilon_3) \equiv (\epsilon_0, \epsilon_1, -\epsilon_2, -\epsilon_3) \equiv (-\epsilon_0, \epsilon_1, -\epsilon_2, \epsilon_3) \equiv (-\epsilon_0, \epsilon_1, \epsilon_2, -\epsilon_3). \tag{2.8}$$

We may therefore without loss of generality fix $\epsilon_0 = 1$, hold $\epsilon_2 > 0$, $\epsilon_3 > 0$, and investigate only the full range of R_m and ϵ_1.

2.3. *The adjoint dynamo problem*

Following Gibson & Roberts (1966) and Kono & Roberts (1991) we define the adjoint problem, $\mathscr{D}^\dagger \boldsymbol{B}^\dagger$, to satisfy

$$\int_V \{\boldsymbol{A}^\dagger \cdot \mathscr{D}\boldsymbol{B} - \boldsymbol{A} \cdot \mathscr{D}^\dagger \boldsymbol{B}^\dagger\} \mathrm{d}V = 0, \tag{2.9}$$

where $\boldsymbol{A}$, $\boldsymbol{A}^\dagger$ are the vector potentials.

Kono & Roberts (1991) showed that the adjoint problem defined in this way can be expressed, for the geometry considered above, as

$$\mathscr{D}^\dagger \boldsymbol{B}^\dagger = \frac{\partial \boldsymbol{B}^\dagger}{\partial t} - R_m \nabla \times (-\boldsymbol{u} \times \boldsymbol{B}^\dagger) + \nabla \times \nabla \times \boldsymbol{B}^\dagger = 0, \tag{2.10a}$$

$$\nabla \times \nabla \times \widehat{\boldsymbol{B}}^\dagger = 0, \qquad r > 1, \tag{2.10b}$$

$$\nabla \times \widehat{\boldsymbol{B}}^\dagger = O(r^{-3}), \qquad r \to \infty, \tag{2.10c}$$

$$\nabla \times \boldsymbol{B}^\dagger = \nabla \times \widehat{\boldsymbol{B}}^\dagger, \qquad r = 1. \tag{2.10d}$$

Expanding $\boldsymbol{B}^\dagger$ in terms of poloidal and toroidal spherical harmonics, the matching condition (2.10*d*) gives

$$\frac{\mathrm{d}T_l^{m\dagger}}{\mathrm{d}r} + \frac{l}{r} T_l^{m\dagger} = 0, \qquad S_l^{m\dagger} = 0, \qquad r = 1. \tag{2.11}$$

Therefore the equation for the adjoint field $\boldsymbol{B}^\dagger$ in the sphere V is identical to the equation for a physical field except for a change in sense of the velocity, $\boldsymbol{u} \to -\boldsymbol{u}$. $\boldsymbol{B}^\dagger$ must, however, satisfy quite different boundary conditions, the condition required of adjoint toroidal harmonics corresponding to that of physical poloidal harmonics, and vice versa (cf. equation (2.3)).

If the boundary were to play only a secondary role in the problem, we might expect the physical system with velocity $-\boldsymbol{u}$ to possess a solution similar to that of the adjoint system, and thus of similar eigenvalue to the solution obtained for velocity $\boldsymbol{u}$. Such a situation, where velocities of opposite sense are capable of exciting dynamos with almost equal ease, has long been observed in the $\alpha\omega$-dynamo literature (e.g. Roberts 1972). In trying to explain this result, Proctor (1977*a*, *b*) considered a 'comparison' system, identical to the dynamo system but for the artificially prescribed boundary conditions

$$T = 0, \qquad S = 0, \qquad r = 1. \tag{2.12}$$

Proctor established that this system possesses identical eigenvalues for the two velocities $\boldsymbol{u}$ and $-\boldsymbol{u}$, the adjoint of this system differing from the original only in terms of such a velocity mapping, the boundary conditions in both cases being homogeneous. Furthermore, he could show that an E^A solution for velocity $\boldsymbol{u}$ was related to an E^S solution for velocity $-\boldsymbol{u}$, and vice versa, which is the case approximately observed for $\alpha\omega$-dynamos. Although the comparison system allows this result to be established, the artificial boundary conditions imposed mean that its physical relevance is not immediately obvious. The deviation from the physical problem can, however, be investigated by considering a system where the fluid region is surrounded by a quiescent shell of identical conductivity, constituting the region $1 < r < d$. For $d \gg 1$ it is obvious that the influence of the artificial boundary condition is reduced, and the system approximates a true dynamo surrounded by a quiescent conducting layer.

Such a dynamo system has previously been considered by Hutcheson & Gubbins (1994), who showed that, in the stationary case, the matching condition for $\boldsymbol{B}$ gives

$$\frac{\mathrm{d}T_l^m}{\mathrm{d}r} + f(d,l)T_l^m = 0, \qquad \frac{\mathrm{d}S_l^m}{\mathrm{d}r} + \frac{l}{r}S_l^m = 0, \qquad r = 1, \tag{2.13a}$$

$$f(d,l) = \left(l + \frac{l+1}{d^{2l+1}}\right) \Big/ \left(1 - \frac{1}{d^{2l+1}}\right). \tag{2.13b}$$

The condition appropriate to the comparison system can be similarly calculated to be

$$\frac{\mathrm{d}T_l^m}{\mathrm{d}r} + f(d,l)T_l^m = 0, \qquad \frac{\mathrm{d}S_l^m}{\mathrm{d}r} + f(d,l)S_l^m = 0, \qquad r = 1. \tag{2.14}$$

The conditions for both systems reduce to

$$\frac{\mathrm{d}T_l^m}{\mathrm{d}r} + \frac{l}{r}T_l^m = 0, \qquad \frac{\mathrm{d}S_l^m}{\mathrm{d}r} + \frac{l}{r}S_l^m = 0, \qquad r = 1, \tag{2.15}$$

as $d \to \infty$; in this limit, therefore, the dynamo system must also obey the exact $E^S \leftrightarrow E^A$ eigenvalue symmetry under $\boldsymbol{u} \leftrightarrow -\boldsymbol{u}$.

Proctor (1977*b*) showed that the differences in eigenvalues between dynamo and comparison systems will be at most $O(d^{-3})$; these arguments are considered further in §4, where numerical calculations are carried out in an attempt to explore the eigenvalue symmetry and to quantify the effect of the insulating boundary on dynamo action.

2.4. *The Braginsky limit*

Whilst we are primarily interested in obtaining three-dimensional (3D) solutions, the Earth's core is expected to have R_m of order 10^2–10^4 (e.g. Melchior 1986),

making the high-R_m asymptotic analysis of Braginskiĭ (1964*a*) of relevance. The axisymmetric Braginsky limit (which term, along with 'the asymptotic limit', we will use to denote the limit investigated by Braginskiĭ 1964*a*, as summarized below) allows much finer numerical resolution (for comparable computational cost) than the 3D system, and so can help in directing and comprehending 3D calculations. In view of past numerical difficulties with such calculations, this simpler analogue system can also give us greater confidence in the numerical validity of our results.

Braginskiĭ (1964*a*) considered the limit $R_m \gg 1$, with fluid velocity and magnetic field ordered, in cylindrical coordinates (s, ϕ, z), as

$$\boldsymbol{u}(s,\phi,z) = u(s,z)\boldsymbol{e}_\phi + R_m^{-1}\boldsymbol{u}_p(s,z) + R_m^{-1/2}\boldsymbol{u}'(s,\phi,z), \tag{2.16a}$$

$$\boldsymbol{B}(s,\phi,z) = B(s,z)\boldsymbol{e}_\phi + R_m^{-1}\boldsymbol{B}_p(s,z) + R_m^{-1/2}\boldsymbol{B}'(s,\phi,z), \tag{2.16b}$$

where $u(s,z)\boldsymbol{e}_\phi$, $B(s,z)\boldsymbol{e}_\phi$ are the azimuthal axisymmetric components, $\boldsymbol{u}_p(s,z)$, $\boldsymbol{B}_p(s,z)$ the poloidal axisymmetric components, and $\boldsymbol{u}'(s,\phi,z)$, $\boldsymbol{B}'(s,\phi,z)$ the non-axisymmetric fields. $\boldsymbol{B}_p$ is given by scalar $A(s,z)$ via $\boldsymbol{B}_p = \nabla \times (A\boldsymbol{e}_\phi)$.

Considering the azimuthally averaged induction equation to leading order in $R_m^{-1/2}$ gives

$$\frac{\partial \boldsymbol{B}_e}{\partial t} = \nabla \times (\boldsymbol{u}_e \times \boldsymbol{B}_e) + \nabla \times (\alpha B \boldsymbol{e}_\phi) + \nabla^2 \boldsymbol{B}_e, \tag{2.17a}$$

in terms of the 'effective' quantities,

$$\boldsymbol{B}_e = B\boldsymbol{e}_\phi + \nabla \times (A_e \boldsymbol{e}_\phi), \tag{2.17b}$$

$$A_e = A + \tfrac{1}{2}s\langle\{\boldsymbol{v}_p \times \widehat{\boldsymbol{v}}_p\}_\phi\rangle B, \tag{2.17c}$$

$$\boldsymbol{u}_e = u\boldsymbol{e}_\phi + \boldsymbol{u}_{ep}, \tag{2.17d}$$

$$\boldsymbol{u}_{ep} = \boldsymbol{u}_p + \nabla \times \left(u\tfrac{1}{2}s\langle\{\boldsymbol{v}_p \times \widehat{\boldsymbol{v}}_p\}_\phi\rangle \boldsymbol{e}_\phi\right), \tag{2.17e}$$

where

$$\alpha = \frac{1}{s}\left\langle \{\boldsymbol{v}_p \times \widehat{\boldsymbol{v}}_p\}_\phi + \left\{\boldsymbol{v}_p \times \frac{\partial_1 \boldsymbol{v}_p}{\partial\phi}\right\}_\phi \right\rangle + 2\langle(\nabla_p r v_r)\cdot\nabla_p \widehat{v}_z\rangle. \tag{2.17f}$$

In the above

$$\boldsymbol{v}_p = \boldsymbol{u}_p'/u, \tag{2.17g}$$

angle brackets denote an azimuthal averaging, $\partial_1/\partial\phi$ differentiation with respect to ϕ treating unit vectors as constants, and the hat the inverse operation of indefinite integration with respect to ϕ, the inverse of $\partial_1/\partial\phi$.

We use α for Braginsky's Γ for consistency with recent notation. Equation (2.17*a*) is the axisymmetric $\alpha\omega$-equation commonly studied in MHD, except in terms of the effective fields defined above.

For the KR velocity, Braginsky's scalings can be reproduced by fixing $\epsilon_0 = 1$, and considering the limit

$$\epsilon_1 \to 0, \qquad R_m \to \infty, \qquad \bar{\epsilon}_1 = \epsilon_1 R_m = \text{constant}, \tag{2.18a}$$

$$\epsilon_2 \to 0, \qquad \epsilon_3 \to 0, \qquad R_m \to \infty, \qquad \bar{\epsilon}_2\bar{\epsilon}_3 = \epsilon_2\epsilon_3 R_m = \text{constant}, \tag{2.18b}$$

whilst keeping

$$\epsilon_1/(\epsilon_2\epsilon_3) = \bar{\epsilon}_1/(\bar{\epsilon}_2\bar{\epsilon}_3) = \text{constant}. \tag{2.18c}$$

Following KR, the prescriptions given by (2.17*d*) and (2.17*f*) give

$$\boldsymbol{u}_{ep} = \bar{\epsilon}_1 \boldsymbol{u}_p + \bar{\epsilon}_{1e} \boldsymbol{s}_2^0 + \bar{\epsilon}_{4e} \boldsymbol{s}_4^0, \tag{2.19a}$$

$$\bar{\epsilon}_{1e} = -\tfrac{3}{7} \bar{\epsilon}_2 \bar{\epsilon}_3 t_1^0 \left(\sigma_2^{2c} \sigma_2^{2s'} - \sigma_2^{2s} \sigma_2^{2c'} \right), \tag{2.19b}$$

$$\bar{\epsilon}_{4e} = \tfrac{9}{70} \bar{\epsilon}_2 \bar{\epsilon}_3 t_1^0 \left(\sigma_2^{2c} \sigma_2^{2s'} - \sigma_2^{2s} \sigma_2^{2c'} \right), \tag{2.19c}$$

where $\sigma_2^{2c} = s_2^{2c}/t_1^0$, $\sigma_2^{2s} = s_2^{2s}/t_1^0$, and primes indicate differentiation with respect to r;

$$\alpha = \bar{\epsilon}_2 \bar{\epsilon}_3 (A_1 \overline{P}_1^0 + A_3 \overline{P}_3^0), \tag{2.20a}$$

$$A_1 = \tfrac{9}{5} \left[\left(\sigma_2^{2c'} \sigma_2^{2s''} - \sigma_2^{2s'} \sigma_2^{2c''} \right) - \left(\frac{t_1^{0'}}{t_1^0} + \frac{5}{r} \right)' \left(\sigma_2^{2c} \sigma_2^{2s'} - \sigma_2^{2s} \sigma_2^{2c'} \right) \right], \tag{2.20b}$$

$$A_3 = -\tfrac{9}{5} \left[\left(\sigma_2^{2c'} \sigma_2^{2s''} - \sigma_2^{2s'} \sigma_2^{2c''} \right) - \left(\frac{t_1^{0'}}{t_1^0} - \frac{5}{r} \right)' \left(\sigma_2^{2c} \sigma_2^{2s'} - \sigma_2^{2s} \sigma_2^{2c'} \right) \right]. \tag{2.20c}$$

We have here employed Schmidt quasi-normalized associated Legendre functions $\overline{P}_l^m$.

For the KR velocity with a fixed value of p, dynamo action in the asymptotic limit is reduced to a function of a two-dimensional (2D) parameter space, $(\bar{\epsilon}_1, \bar{\epsilon}_2 \bar{\epsilon}_3)$. We may therefore specify $\bar{\epsilon}_1$ and investigate growth rates as a function of $\bar{\epsilon}_2 \bar{\epsilon}_3$; we will most frequently be interested in locating the critical values, $(\bar{\epsilon}_2 \bar{\epsilon}_3)_c$, at which magnetic fields are sustained.

We investigate this limit to guide us in our 3D calculations, and so must translate conclusions back to the latter regime. To do so we must fix a value for $\epsilon_2 \epsilon_3$, keeping its magnitude relatively small so as to remain close enough to the asymptotic limit for correspondence to be anticipated. The remaining freedom in our 3D velocity is then also limited to a 2D parameter space, (ϵ_1, R_m), and a direct mapping from the Braginsky limit can be carried out via (2.18*c*) and either (2.18*a*) or (2.18*b*), producing extrapolated predictions of R_m^c as a function of ϵ_1.

Justification of such faith in the utility of extrapolations from the asymptotic limit is given by suites of calculations approaching the limit explicitly, such as those carried out by KR. The axisymmetric magnetic field morphology also agrees well between solutions of the two systems. A good correspondence between the Braginsky limit and the nearby 3D regime has been obtained for all solutions presented here.

2.5. *Numerical methods*

We adopt the numerical method of Bullard & Gellman (1954), as implemented by Gubbins (1973), with the modifications to the boundary conditions outlined above. Thus we have the infinite set of coupled equations to be solved in V,

$$\frac{\partial T_\gamma}{\partial t} = \nabla_\gamma^2 T_\gamma + \frac{R_m}{r^2} \sum_{\alpha,\beta} \left[(s_\alpha S_\beta T_\gamma) + (t_\alpha S_\beta T_\gamma) + (s_\alpha T_\beta T_\gamma) + (t_\alpha T_\beta T_\gamma) \right], \tag{2.21a}$$

$$\frac{\partial S_\gamma}{\partial t} = \nabla_\gamma^2 S_\gamma + \frac{R_m}{r^2} \sum_{\alpha,\beta} \left[(s_\alpha S_\beta S_\gamma) + (t_\alpha S_\beta S_\gamma) + (s_\alpha T_\beta S_\gamma) + (t_\alpha T_\beta S_\gamma) \right], \tag{2.21b}$$

where $\nabla_\gamma^2 = \partial^2/\partial r^2 - l_\gamma(l_\gamma + 1)/r^2$, the greek subscripts being shorthand for the spherical harmonics involved, and where the interaction notation is such that $(t_\alpha T_\beta S_\gamma)$ represents the production of poloidal magnetic field from toroidal via induction by a toroidal velocity; the detailed form of these terms, linear in the unknowns and in their first and second derivatives, is given by Bullard & Gellman (1954). An analogous formalism is used for the Braginsky limit calculations, the new interactions arising from the α-effect being given by Roberts & Stix (1972).

These equations must be truncated to a finite set, done by restricting the expansion to harmonics with degree $l \leqslant L$. A uniform radial grid of N points spaced as $h = 1/N$ is imposed, and the radial derivatives are approximated by second-order finite differences, incorporating the appropriate matching conditions at $r = 1$. This yields an algebraic eigenvalue problem, which we then solve via inverse iteration, or (at low truncation) the QR method (see e.g. Press et al. 1989).

Eigenvalues obtained by these algebraic methods are limited to the $O(h^2)$ accuracy of the finite-difference scheme. More accurate values can be obtained via Richardson extrapolation of eigenvalues obtained for two or more different mesh sizes. The $O(h^2)$ and higher error terms can then be eliminated, leading to $O(h^4)$ or more accurate solutions. Eigenvalues obtained in this way were found to agree well with those calculated using the independent parallel shooting method of Conte (1966), here adopted with fourth-order Runge–Kutta integration. In addition, the solutions reported by Pekeris et al. (1973), KR, and Dudley & James (1989) have all been successfully reproduced.

Checks such as these cannot, however, give information on the reliability of the convergence of solutions. The truncation of the spherical harmonic expansion at degree L artificially restricts the flow of energy to short length scales, potentially misrepresenting the physical problem. The literature shows that this truncation problem has in the past led to erroneous conclusions.

As noted by Gubbins (1973), the apparent convergence of eigenvalues at relatively low truncation levels is not in itself sufficient indication of a converged solution. Convergence of the eigenvector must be examined either graphically or through the calculation of form-dependent (and hence relatively sensitive) quantities such as the magnetic energy and ohmic dissipation, the calculation of which is considered by Pekeris et al. (1973); these measures must be seen to be consistent from calculations at a range of truncation levels, before confidence may be placed in any solution.

For dynamos in the high-R_m, nearly axisymmetric regime appropriate to Braginsky's analysis, however, agreement between the asymptotic solution and the solution in the nearby 3D regime provides an ideal test of numerical convergence. The asymptotic limit constitutes a numerically independent system approximating the same physical state, and its greater simplicity allows calculations to be carried out to much finer resolution.

An alternative truncation scheme was also adopted to investigate numerical convergence further. Here we incorporate only harmonics satisfying

$$l + m \leqslant L_\Delta; \tag{2.22}$$

this scheme, referred to as triangular truncation, and successfully applied in other contexts (e.g. Zhang & Busse 1987), allows the behaviour of long azimuthal wavelength modes to be explored to greater resolution at the expense of the short azimuthal wavelength modes. Although clearly not of universal use, the predominance of energy in the low-m modes, observed in the solutions detailed below, allowed this method to be adopted with negligible loss of accuracy.

The numerical difficulties encountered should not be underestimated, as they arise from the very nature of the problem addressed, whether a self-sustaining magnetic field solution exists. For R_m below a certain minimum value, all solutions must decay with time (e.g. Roberts & Gubbins 1987). Increasing R_m is essential in order to find dynamo action, but this decreases the length scale of the magnetic field as the smoothing effects of diffusion are reduced, and will ultimately cause any numerical scheme to fail through lack of spatial resolution.

Thus there are only two possible outcomes from a calculation:

(*a*) a self-sustaining magnetic field is found, with corresponding R_m^c, which appears to converge satisfactorily according to the criteria outlined above;

(*b*) we are unable to find marginally stable solutions for values of R_m less than some upper limit set by the numerical scheme.

We can never assert that a given flow fails to excite a dynamo, as the behaviour at higher R_m remains unknowable.

3. Variations in solutions obtained for varying velocity parameters

3.1. *The role of meridional circulation*

Meridian circulation was shown by Roberts (1972) to play an important role in determining the time-dependence of $\alpha\omega$-dynamos. Its importance for the KR velocity was investigated through varying the parameter ϵ_1, holding other parameters constant. The radial complexity of the convective cells was fixed at three cells ($p = 3\pi$), this value providing a relatively large-scale laminar flow yet allowing for well-converged solutions (increasing p increases the ease with which dynamo action is obtained, and the ease of numerical convergence, as shown in §3.2). The strength of the convection was fixed at $\epsilon_2 = \epsilon_3 = 0.04$.

Before considering the 3D results, we examine the Braginsky limit system, whose simplicity facilitates thorough investigation. Marginal stability curves for this system are shown in figure 1. The range $-300 < \bar{\epsilon}_1 < 300$ is considered, and solutions for both signs of $\bar{\epsilon}_2\bar{\epsilon}_3$ are shown, for $|\bar{\epsilon}_2\bar{\epsilon}_3| \leqslant 100$. The solution investigated by KR is marked KR. Points A–F, giving the most easily excited modes of $E^A P_2^S$ and $E^S P_2^S$ symmetry at $\epsilon_1 = -250$, 0, 250 for $\bar{\epsilon}_2\bar{\epsilon}_3 > 0$ are marked for future reference; likewise points G–L, for $\bar{\epsilon}_2\bar{\epsilon}_3 < 0$. The numerical convergence of these solutions is good; calculations for these 12 points have been conducted to degree $L = 32$, giving eigenvalue convergence to 6 significant figures.

The solution branch located by KR ($E^A P_2^S$, $\bar{\epsilon}_1 > 0$, $\bar{\epsilon}_2\bar{\epsilon}_3 > 0$) can be seen in relation to the wider range of solutions obtained. The overall picture is complicated – with, for example, bifurcations from stationary to oscillatory solutions at the approximate points $(\bar{\epsilon}_1, \bar{\epsilon}_2\bar{\epsilon}_3) = (-197, 83), (-80, 58), (96, -64), (155, -75)$ – but the behaviour of the most easily excited modes is relatively straightforward. With no meridional circulation, oscillatory solutions are preferred; with the addition of meridional circulation in either sense, stationary solutions become more easily excited, and, for the 'correct' sense of $\bar{\epsilon}_1$, possess considerably smaller critical values of $\bar{\epsilon}_2\bar{\epsilon}_3$. This behaviour is consistent with the conclusions of Roberts (1972) on the behaviour of quite general, arbitrary, $\alpha\omega$ systems.

E^A solutions tend to be the more easily excited symmetry for $\bar{\epsilon}_2\bar{\epsilon}_3 > 0$, whilst for $\bar{\epsilon}_2\bar{\epsilon}_3 < 0$, E^S solutions are preferred; the mapping $\bar{\epsilon}_1 \to -\bar{\epsilon}_1$, $\bar{\epsilon}_2\bar{\epsilon}_3 \to -\bar{\epsilon}_2\bar{\epsilon}_3$ (physically identifiable with $\boldsymbol{u} \to -\boldsymbol{u}$) approximately transposes an E^A solution for an E^S solution and vice versa. Again, this is consistent with Roberts (1972), and is as anticipated from considerations of the adjoint system outlined in §2.3.

This picture is clear for the Braginsky limit; we are, however, interested in non-axisymmetric solutions at finite R_m. Extrapolating the above results to the case $\epsilon_2 = \epsilon_3 = 0.04$ using (2.18*a*)–(2.18*c*), we obtain the predicted behaviour given in figure 2. The points A–L correspond to the solutions marked on the earlier figure. (For clarity, only the most easily excited solution branches have been shown here.)

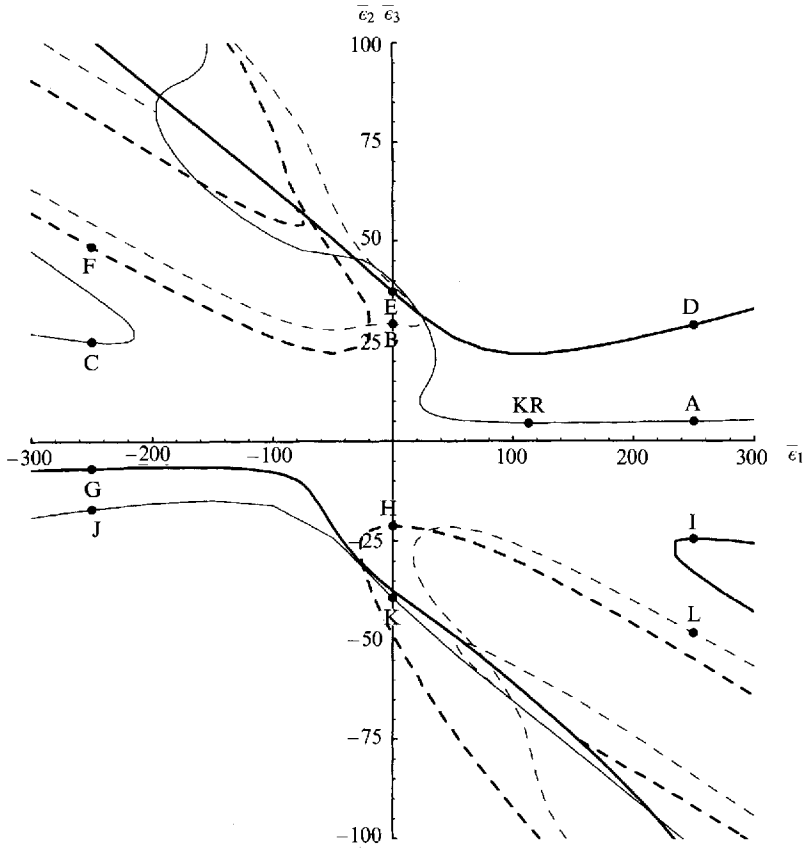

FIGURE 1. Critical stability curves $\bar{\epsilon}_2\bar{\epsilon}_3$ with $\bar{\epsilon}_1$, for the Braginsky limit system with $p = 3\pi$, at truncation level $(L, N) = (14, 40)$. Thin (thick) lines denote E^A (E^S) solutions; solid (dashed) lines denote stationary (oscillatory) solutions. Points A–L and KR are referred to in the text.

Figure 3 shows the true variation of R_m^c with ϵ_1 for 3D calculations with $\epsilon_2 = \epsilon_3 = 0.04$, conducted at truncation level $(L, N) = (14, 150)$. This figure details only solution branches that are most easily excited for some value of ϵ_1; the convergence of other solutions, with critical values at higher R_m, was not deemed good enough to warrant extensive calculations, even at this resolution. In all essential details this plot concurs with figure 2, highlighting the utility of Braginsky's high-R_m limit.

To allow a more complete range of solutions to be considered and to verify convergence more thoroughly, the solutions corresponding to the isolated points A–L were investigated in more detail, employing the triangular truncation scheme of (2.22) for resolutions (L_Δ, N) up to $(24, 150)$; the results are given in table 2. For solutions at lower R_m^c, convergence is quite satisfactory. For those of higher R_m^c (points E, F, K, L), the convergence is poorer, but still acceptable. Furthermore, in all twelve cases the agreement of solution morphology between the 3D and the Braginsky limit calculations gives every reason for confidence in even the least well converged of these solutions.

All these solutions remain within the high-R_m, nearly axisymmetric regime, the bulk of the magnetic energy in each case lying in the axisymmetric components of the field. The morphology of this part of the field is shown in figures 4–6 for the 3D solutions A, B, C, F, given in table 2, illustrating the most easily excited solution

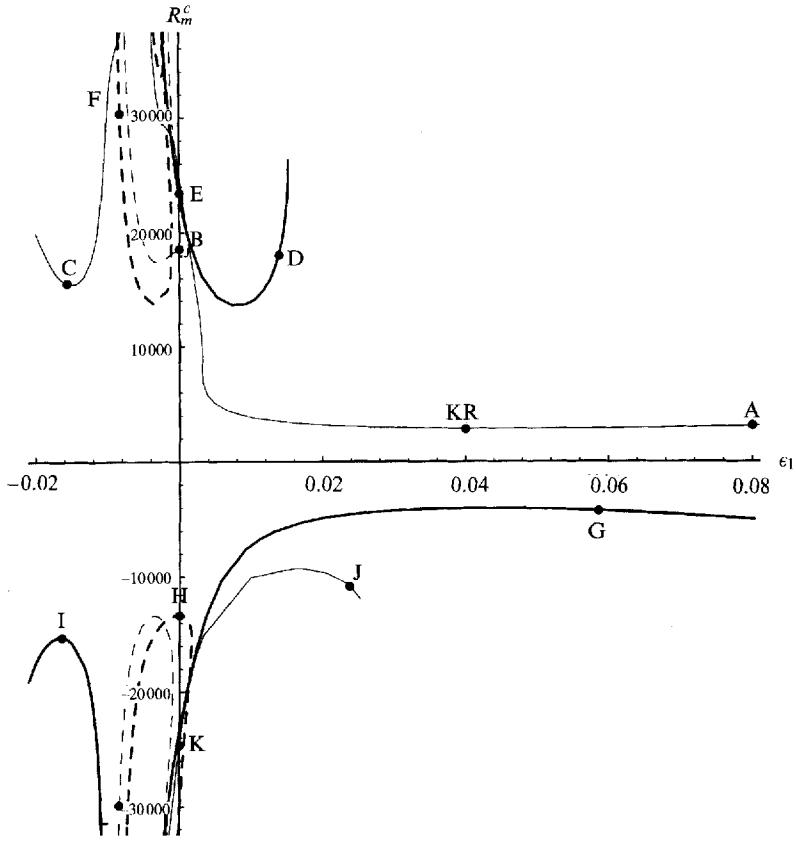

FIGURE 2. Predicted R_m^c variations for $\epsilon_2 = \epsilon_3 = 0.04$, from extrapolation of Braginsky limit results for $p = 3\pi$ at $(L, N) = (14, 40)$. Points A–L and KR refer to the corresponding solutions in figure 1; line types are as for that figure.

branches obtained with varying ϵ_1 for $R_m > 0$. We show the axisymmetric toroidal field B_ϕ, and a 'streamfunction' for the axisymmetric poloidal field, F_ϕ, given by $F_\phi = \sin\theta\, \mathrm{d}S(r, \theta, \phi)/\mathrm{d}\theta$, analogous to the streamfunction used by Zhang & Busse (1987).

The oscillatory behaviour of solutions B and F consists of the cyclical appearance and migration of bundles of magnetic flux: a manifestation of the dynamo-wave mechanism familiar in $\alpha\omega$-models (see, e.g. Parker 1979). The migration observed is poleward for the solutions shown, where $R_m > 0$, and is equatorward for the solutions obtained for $R_m < 0$, consistent with the conclusions of Roberts (1972) for $\alpha\omega$-models.

Figures 7–9 show the radial magnetic field B_r, at $r = 1$, for the same solutions. This quantity constitutes the field visible to an external observer, and thus is of use for comparisons with the magnetic fields of planetary bodies. These plots illustrate the nearly axisymmetric nature of the solutions; very little energy can be seen in azimuthal wavenumbers $m > 2$. For the oscillatory solutions, the migration of flux is once more evident in the flux observed at the surface of the dynamo region.

The stationary E^A solution located by KR can now be seen as only one of a variety of possible solutions for the general KR velocity, with meridional circulation being a critical factor in controlling the solution physically preferred. This variation explains the inability of Hutcheson & Gubbins (1994) to locate a stationary E^A dynamo for

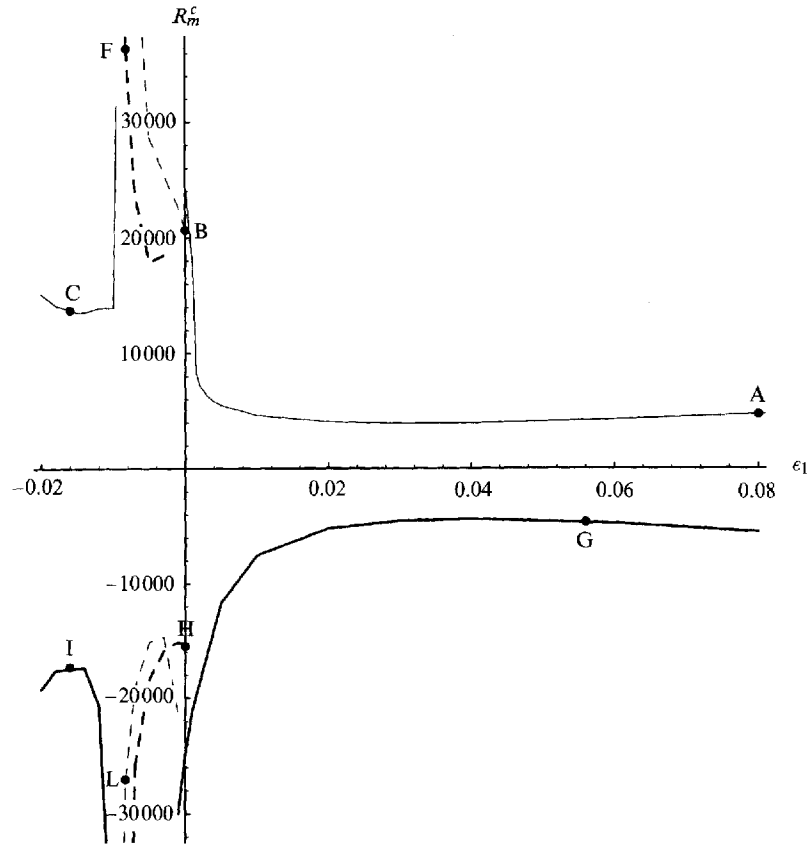

FIGURE 3. True R_m^c variation for $\epsilon_2 = \epsilon_3 = 0.04$, for $p = 3\pi$ at $(L, N) = (14, 150)$. Line types are as for figure 1.

the Lilley ($\epsilon_1 = 0$) case of the $p = 3\pi$ KR velocity, the most easily excited E^A field in this case being oscillatory.

E^S fields are in general equally easily excited as E^A fields, the solutions again displaying the approximate symmetry under $\boldsymbol{u} \rightarrow -\boldsymbol{u}$ (reflection in the x-axis in figures 2 and 3), discussed in §2.3; this symmetry is further investigated in §4.

To some extent the changes in field morphology obtained for varying meridional circulation can be understood through simple considerations of flux advection. Gubbins (1993) and Hutcheson & Gubbins (1994) have previously related the regions of surface flux concentration in KR dynamos to regions of downwelling of the non-axisymmetric flow. This argument derives from consideration of the frozen-flux (i.e. infinite R_m) limit, where radial field is carried in flux bundles by flow tangential to the surface, and concentrated where the flow ultimately downwells; given the high values of R_m associated with Braginsky regime dynamos, it seems reasonable that a similar behaviour be observed. Thus solution A, with a positive sense of meridional circulation (corresponding to upwelling at the poles), has its principle flux concentrations offset from the poles, whilst solution C, for $\epsilon_1 < 0$ (polar downwelling) has a greater concentration of flux at high latitudes (figure 7).

The value of ϵ_1 has been kept small in the preceding, to remain within the Braginsky regime. Figure 3, however, shows that the E^A solutions obtained for $\epsilon_1 > 0$ remain easily excited to higher values of ϵ_1. As ϵ_1 increases further however, this

solution branch becomes less easily excited, and convergence deteriorates. Plots of the axisymmetric field associated with solutions for increasing ϵ_1 (figure 10) show why this is the case: the increasing meridional circulation expels the toroidal field from the interior, in the manner associated with flows with closed streamlines investigated by Weiss (1966). The toroidal field, being unable to penetrate to the insulating region $\hat{V}$, remains concentrated at the boundary, resulting in high ohmic dissipation, ultimately prohibitive to dynamo action. A similar effect was first seen in dynamos with axisymmetric flows by Bullard & Gubbins (1977).

3.2. *The radial complexity of the convective cells*

The complexity of fluid motion necessary for dynamo action is a point of some interest to dynamo theory, some degree of complexity being required from the numerous anti-dynamo theorems – and being anticipated to facilitate more efficient field production via the various α-effect analyses – yet large-scale laminar flows being anticipated to be energetically preferable. For the KR velocity, the effect of the radial complexity of the convective motions can be investigated through varying p.

Figure 11 shows the critical dynamo curves obtained in the Braginsky limit with $p = \pi, 2\pi, 3\pi, 4\pi$, for both signs of $\bar{\epsilon}_2\bar{\epsilon}_3$ and for $-300 < \bar{\epsilon}_1 < 300$. The broad features obtained in each case are similar, the role of meridional circulation and the importance of the sign of $\bar{\epsilon}_2\bar{\epsilon}_3$, investigated in the preceding section, being verified for each p. There are two obvious variations of importance, however. First, the critical values of $\bar{\epsilon}_2\bar{\epsilon}_3$ decrease markedly as p increases; this was to have been expected from the dependence of the regenerative term α on the parameter p, given by (2.20), which, for the KR velocity transcribed via $\sigma_2^{2s} = g(r)\cos pr$, $\sigma_2^{2c} = g(r)\sin pr$, depends on the simple forms

$$\sigma_2^{2c}\sigma_2^{2s'} - \sigma_2^{2s}\sigma_2^{2c'} = -pg^2, \tag{3.1}$$

$$\sigma_2^{2c'}\sigma_2^{2s''} - \sigma_2^{2s'}\sigma_2^{2c''} = p(gg'' - 2g'^2 - p^2g^2). \tag{3.2}$$

Secondly, increasing p shifts the whole pattern of critical curves towards more positive values of $\bar{\epsilon}_1$; again this could have been expected from the analysis of Braginsky, the effective meridional circulation given by (2.19), again, by the above, depending relatively simply upon p. The contribution of the convective cells to the meridional circulation is therefore of importance, with the result that, for example, the Lilley ($\epsilon_1 = 0$) case favours a stationary field for the large-scale flow $p = \pi$, but an oscillatory field for $p = 3\pi$.

As large-scale laminar flows are anticipated to be energetically favoured, the case $p = \pi$ is investigated in more detail. Figure 12 shows the critical dynamo curves anticipated for $\epsilon_2 = \epsilon_3 = 0.04$, extrapolated from Braginsky limit solutions as before. Again points A–L, corresponding to the most easily excited solutions at $\bar{\epsilon}_1 = -250, 0, 250$, are marked. As was the case with $p = 3\pi$, the convergence of the Braginsky limit solutions is again good. The high values of R_m^c associated with the $p = \pi$ solutions unfortunately make the convergence of the corresponding 3D solutions poor, and reasonable approximations to all these solutions could not be obtained at the numerical resolution currently possible; the most-easily excitable solutions are attainable however, and figure 13 shows the critical curves obtained for these solutions at $(L, N) = (16, 150)$; table 3 illustrates the convergence of the solutions A, B, G, H, for triangular truncation levels up to $(L_\Delta, N) = (24, 150)$. The axisymmetric field associated with these solutions is shown in figure 14; variations in morphology with ϵ_1 are consistent with that obtained in the preceding section.

The E^A field obtained in the Lilley case, point B, is indeed found to be stationary, in

Point A: E^A, $\epsilon_1 = 0.080$ (Brag. limit $\Rightarrow$ 3090)

$L_\Delta \backslash N$	100	150	$O(h^4)$
14	4645.66	4671.34	4691.89
16	4652.63	4678.22	4698.69
18	4651.78	4677.46	4698.00
20	4651.96	4677.59	4698.10
22	4651.99	4677.63	4698.15
24	4651.95	4677.59	4698.11

Point B: E^A, $\epsilon_1 = 0$ (Brag. limit $\Rightarrow$ 18500(25))

$L_\Delta \backslash N$	100	150	$O(h^4)$
14	18720 (11.27)	19420 (11.49)	19980 (11.67)
16	18600 (13.68)	19540 (14.37)	20290 (14.92)
18	19090 (12.24)	20580 (12.64)	21770 (12.96)
20	19090 (12.23)	20610 (12.64)	21830 (12.97)
22	19090 (12.25)	20610 (12.69)	21830 (13.04)

Point C: E^A, $\epsilon_1 = -0.016$ (Brag. limit $\Rightarrow$ 16100)

$L_\Delta \backslash N$	100	150	$O(h^4)$
14	11661.0	11638.5	11620.5
16	—	—	—
18	14702.1	14890.9	15041.9
20	15073.6	15393.9	15650.2
22	15021.1	15314.8	15549.6
24	15026.0	15322.6	15559.8

Point D: E^S, $\epsilon_1 = 0.014$ (Brag. limit $\Rightarrow$ 18000)

$L_\Delta \backslash N$	100	150	$O(h^4)$
14	16404.1	19195.8	21429.2
16	16699.0	19491.9	21726.2
18	16702.8	19519.6	21773.1
20	16744.2	19594.0	21873.9
22	16734.3	19555.1	21811.8
24	16737.8	19565.3	21827.3

Point E: E^S, $\epsilon_1 = 0$ (Brag. limit $\Rightarrow$ 23500)

$L_\Delta \backslash N$	100	150	$O(h^4)$
14	21614.8	22322.3	22888.3
16	21312.0	22025.6	22596.5
18	21617.6	22480.0	23169.8
20	21647.6	22487.9	23160.2
22	21611.9	22438.6	23100.1
24	21610.7	22435.4	23095.1

Point F: E^S, $\epsilon_1 = -0.0082$ (Brag. limit $\Rightarrow$ 30400(117))

$L_\Delta \backslash N$	100	150	$O(h^4)$
14	38760 (155.1)	38170 (140.0)	37700 (127.9)
16	43910 (139.1)	33710 (115.9)	25550 (97.34)
18	42880 (156.2)	36320 (131.5)	31070 (111.7)
20	—	45580 (147.5)	—
22	—	46890 (147.1)	—

TABLE 2. Continued on facing page.

contrast to the situation for $p = 3\pi$, so the importance of the effective meridional circulation arising from the non-axisymmetric velocity, influencing the time-dependence in the same way as the 'true' (axisymmetric) meridional circulation, is verified. Hutcheson & Gubbins (1994) obtained a similar solution for this case ($p = \pi$, $\epsilon_1 = 0$) upon the addition of a quiescent conducting layer of the type considered in §4, but

Point G: E^S, $\epsilon_1 = 0.056$ (Brag. limit $\Rightarrow -4270$)

$L_A \backslash N$	100	150	$O(h^4)$
14	−4727.37	−4648.48	−4585.37
16	−4701.87	−4626.19	−4565.65
18	−4710.57	−4633.68	−4572.16
20	−4707.17	−4630.77	−4569.65
22	−4708.14	−4631.58	−4570.34
24	−4707.81	−4631.31	−4570.11

Point H: E^S, $\epsilon_1 = 0$ (Brag. limit $\Rightarrow -13300(32)$)

$L_A \backslash N$	100	150	$O(h^4)$
14	−17340 (33.02)	−15610 (33.54)	−14230 (33.96)
16	−16960 (33.64)	−15310 (33.30)	−13990 (33.03)
18	−17140 (33.64)	−15330 (33.35)	−13880 (33.12)
20	−17170 (33.63)	−15350 (33.36)	−13890 (33.14)
22	−17160 (33.63)	−15350 (33.36)	−13900 (33.14)

Point I: E^S, $\epsilon_1 = -0.016$ (Brag. limit $\Rightarrow -15300$)

$L_A \backslash N$	100	150	$O(h^4)$
14	—	—	—
16	—	—	—
18	−21663.8	−18387.8	−15766.9
20	—	−19065.6	—
22	—	−18950.3	—
24	—	−18965.5	—

Point J: E^A, $\epsilon_1 = 0.024$ (Brag. limit $\Rightarrow -10500$)

$L_A \backslash N$	100	150	$O(h^4)$
14	—	—	—
16	−12524.5	−11778.8	−11182.3
18	−13036.1	−11979.4	−11134.0
20	−13048.1	−12031.3	−11217.9
22	−13040.7	−12014.4	−11193.4
24	−13066.3	−12028.0	−11197.3

Point K: E^A, $\epsilon_1 = 0$ (Brag. limit $\Rightarrow -24700$)

$L_A \backslash N$	100	150	$O(h^4)$
14	—	−25205.7	—
16	−25823.0	−25152.8	−24616.6
18	−27095.2	−26362.6	−25776.5
20	−26806.0	−26174.7	−25669.7
22	−26726.8	−26091.3	−25582.9
24	−26739.1	−26102.1	−25592.4

Point L: E^A, $\epsilon_1 = -0.0084$ (Brag. limit $\Rightarrow -29900(117)$)

$L_A \backslash N$	100	150	$O(h^4)$
14	−24940 (108.3)	−26510 (110.2)	−27770 (111.7)
16	−27010 (111.4)	−27940 (110.1)	−28680 (109.1)
18	−27260 (113.0)	−28970 (115.0)	−30340 (116.6)
20	−27840 (113.9)	−29860 (115.8)	−31480 (117.3)
22	−27830 (113.6)	−29800 (115.4)	−31380 (116.8)

TABLE 2. Convergence of $R_m^c(\omega, \omega \neq 0)$ eigenvalues of selected 3D solutions, $p = 3\pi$. The solutions chosen approximate the extrapolations of the Braginsky limit solutions given above for $\epsilon_2 = \epsilon_3 = 0.04$. (The eigenvalues anticipated from the extrapolation are given in the header captions). The triangular truncation scheme was used for these calculations, with L_A up to 24 for stationary solutions, 22 for oscillatory solutions.

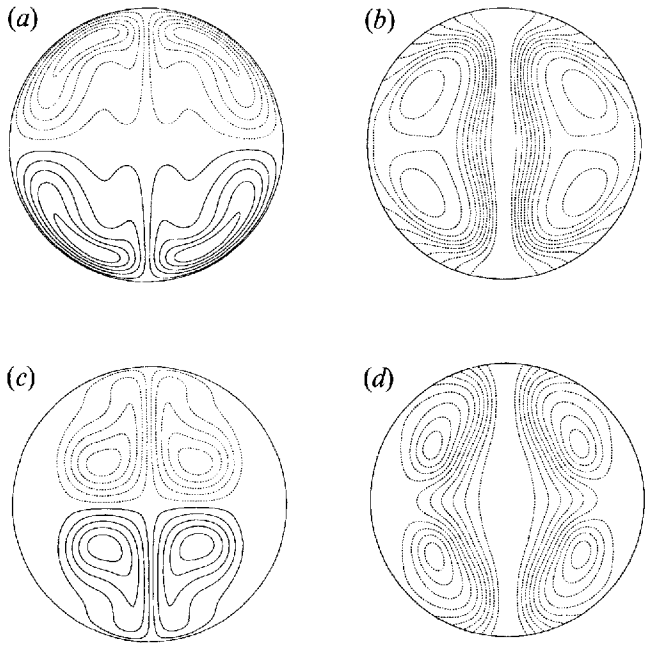

FIGURE 4. The axisymmetric field, in meridional planes, for the marginal stationary $E^A P_2^S$ solutions obtained for $p = 3\pi$, $\epsilon_2 = \epsilon_3 = 0.04$, $R_m > 0$, triangular truncation level $(L_A, N) = (24, 150)$. (*a*) B_ϕ for solution A, $\epsilon_1 = 0.08$, $R_m^c = 4678$, contours from -300 to 300. (*b*) F_ϕ, solution as for (*a*), contours from -1.5 to 0. (*c*) B_ϕ for solution C, $\epsilon_1 = -0.016$, $R_m^c = 15320$, contours from -900 to 900. (*d*) F_ϕ, solution as for (*c*), contours from -1.5 to 0. Both solutions (and all E^A solutions subsequently shown) have been normalized by setting $S_1^0(1) = 1$. All plots employ 11 contour levels, equally spaced between the limits specified; solid (dashed) lines denote positive (negative) values.

could not locate a solution without such a layer. The quiescent layer now appears not to play a critical role: its presence does increase the ease of dynamo action, but the previous failure to locate a regenerative solution in its absence lay simply in the higher value of R_m^c required, making adequate numerical representation beyond the resolution available to earlier studies. The inability of KR to obtain any dynamo solutions for $p \leqslant 2\pi$ can be similarly explained.

We have also investigated solutions for $p > 4\pi$, and obtained consistent behaviour. For slightly greater values of p, the convergence of 3D solutions is improved, the smaller R_m^c values then required decreasing the numerical difficulties encountered; for yet larger p, the numerical representation of the many convective cells becomes increasingly inadequate, and convergence problems are again encountered.

3.3. *The strength of the convective cells*

The previous section considered the influence of the radial complexity of convection on dynamo action, but was restricted to $\epsilon_2 = \epsilon_3 = 0.04$. Here the influence on dynamo action of the latter parameters, controlling the strength of the convective cells, is investigated. Only the regions of the most easily excited stationary solutions obtained for $p = 3\pi$ with $\epsilon_1 = 0.03$ are investigated, but both the E^A solutions obtained for $R_m > 0$ and the E^S solutions for $R_m < 0$ are considered. Results are presented only for $(L, N) = (12, 150)$; these solutions have, however, been confirmed by calculations at higher truncation levels.

Table 4 shows the variation of R_m^c for selected values of ϵ_2 and ϵ_3. R_m^c generally

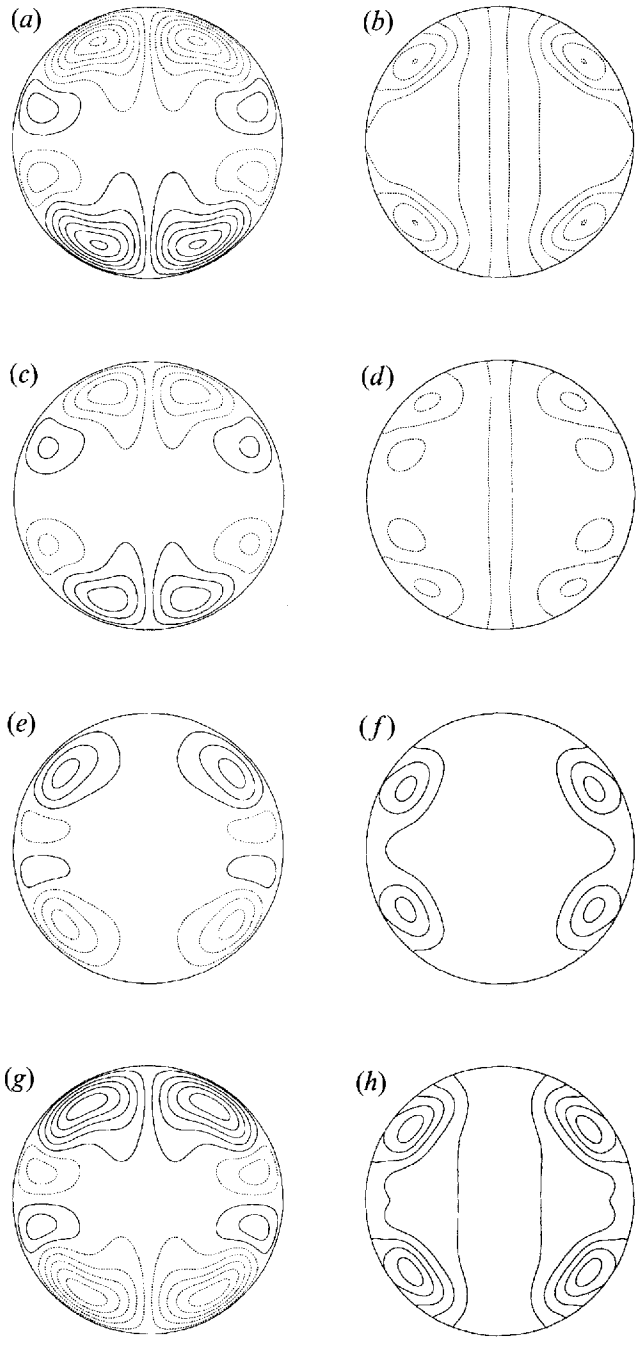

FIGURE 5. The axisymmetric field of the marginal oscillatory $E^A P_2^S$ solution B, with $p = 3\pi$, $\epsilon_1 = 0$, $\epsilon_2 = \epsilon_3 = 0.04$, eigenvalue $R_m^c = 20610$, $\omega = 12.69$ at triangular truncation level $(L_A, N) = (22, 150)$. (*a*), (*c*), (*e*) and (*g*) show B_ϕ at $\omega t = 0$, $\pi/4$, $\pi/2$ and $3\pi/4$ respectively. (*b*), (*d*), (*f*), (*h*) show F_ϕ at the same intervals. Contours of B_ϕ are from -1250 to 1250, of F_ϕ from -1.75 to 0.75. Other details are as for figure 4.

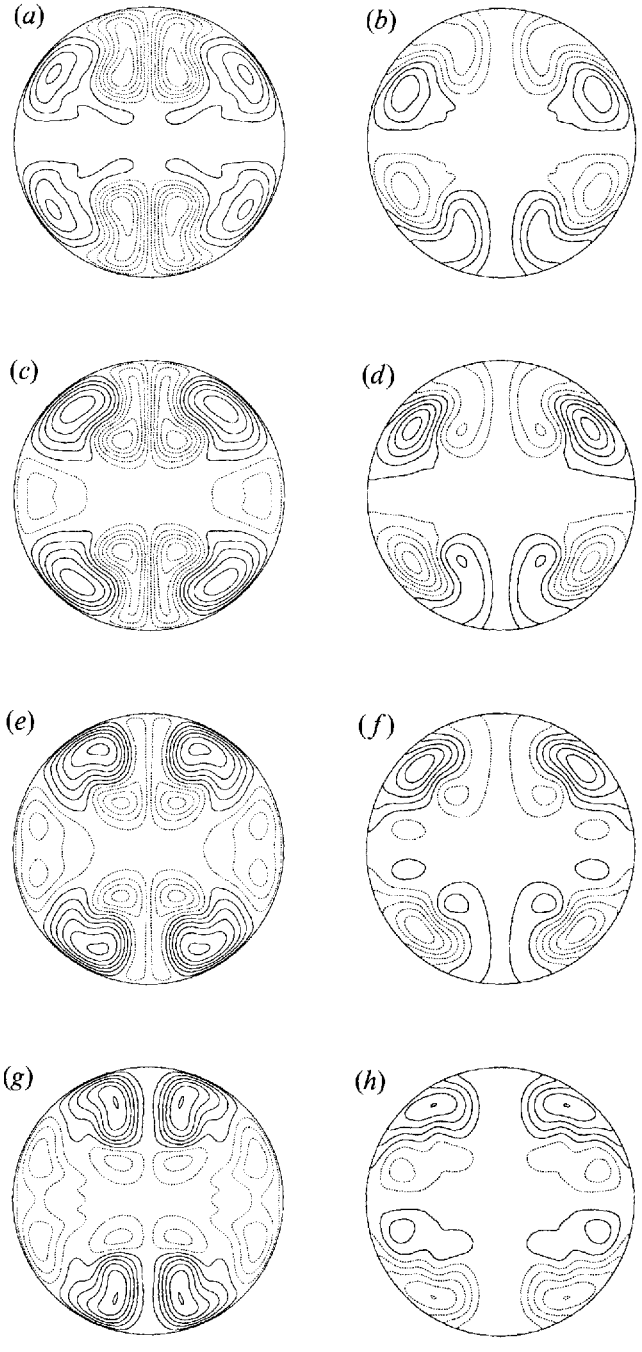

FIGURE 6. The axisymmetric field of the marginal oscillatory $E^S P_2^S$ solution F, with $p = 3\pi$, $\epsilon_1 = -0.0082$, $\epsilon_2 = \epsilon_3 = 0.04$, eigenvalue $R_m^c = 46880$, $\omega = 147.1$ at triangular truncation level $(L_A, N) = (22, 150)$. (*a*), (*c*), (*e*) and (*g*) show B_ϕ at $\omega t = 0$, $\pi/4$, $\pi/2$ and $3\pi/4$ respectively. (*b*), (*d*), (*f*), (*h*) show F_ϕ at the same intervals. The solution has been normalized by setting $\mathrm{Re}\, S_2^0(1) = 1$. Contours of B_ϕ are from -6000 to 6000, of F_ϕ from -5 to 5. Other details are as for figure 4.

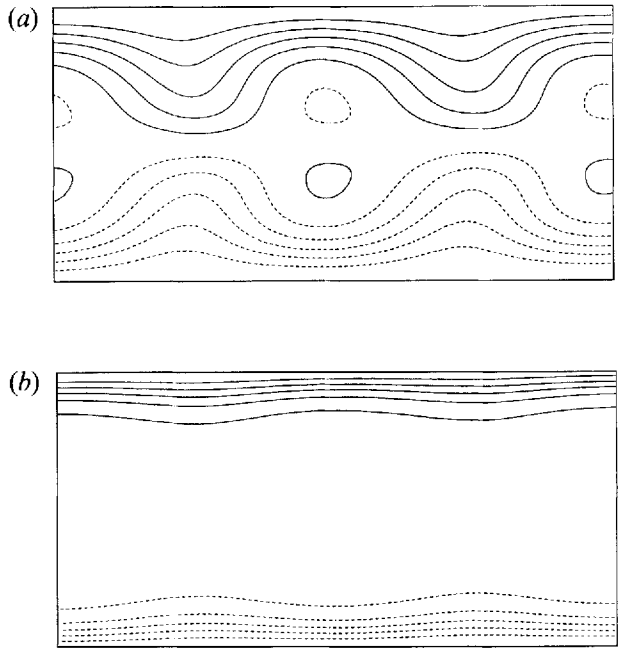

FIGURE 7. The radial field, on cylindrical equidistant projections of the surface $r = 1$, for the marginal stationary $E^A P_2^S$ solutions detailed in figure 4. (*a*) B_r for solution A, contours from -5 to 5. (*b*) B_r for solution C, contours from -17.5 to 17.5. Other details are as for figure 4.

decreases as ϵ_2 and ϵ_3 are increased, as should be anticipated, the convective cells necessary for dynamo action then being enhanced. Figure 15 shows the variation in the form of the field as $\epsilon_2 = \epsilon_3$ is increased from 0.02 to 0.16. It can be seen that the form of the field is in each case similar; the relative magnitudes of the various components of field vary, however, as the deviation from the Braginsky limit increases. Thus axisymmetric field accounts for 99.63% of the magnetic energy (98.50% of the ohmic dissipation) at $\epsilon_2 = \epsilon_3 = 0.02$, dropping to 93.43% (76.07%) at $\epsilon_2 = \epsilon_3 = 0.16$; toroidal field incorporates 99.78% of the magnetic energy (99.25% of the ohmic dissipation) at $\epsilon_2 = \epsilon_3 = 0.02$, 93.83% (90.97%) at $\epsilon_2 = \epsilon_3 = 0.16$.

Clearly, however, even at $\epsilon_2 = \epsilon_3 = 0.16$, the Braginsky limit remains a useful approximation; the field remains predominantly toroidal and axisymmetric, and the morphology of figure 15 remains identifiably that of the corresponding asymptotic solution. Indeed, the variation in the axisymmetric field in these figures can be related to the variations observed with $\bar{\epsilon}_1$ in the limit, since, as $\epsilon_2 = \epsilon_3$ is increased with ϵ_1 held constant, R_m^c decreases, and so $\bar{\epsilon}_1$ decreases. Thus the effect of increasing ϵ_2 and ϵ_3 is comparable with that of decreasing ϵ_1, as long as we remain within the Braginsky regime; figure 15 exhibits variations in morphology comparable with figure 10. This can be understood with reference to figure 16.

As ϵ_2 and ϵ_3 are further increased, deviations from the Braginsky limit continue to increase until convergent solutions capable of producing dynamo action can no longer be obtained.

Deviations from the Braginsky limit are of course non-negligible for the solutions of table 4. This is most obvious in comparisons of solutions with constant product $\epsilon_2\epsilon_3$. In the Braginsky limit, only this product is of import. KR noted, however, that this does not hold for 3D calculations, with 'asymmetry' between ϵ_2 and ϵ_3 affecting

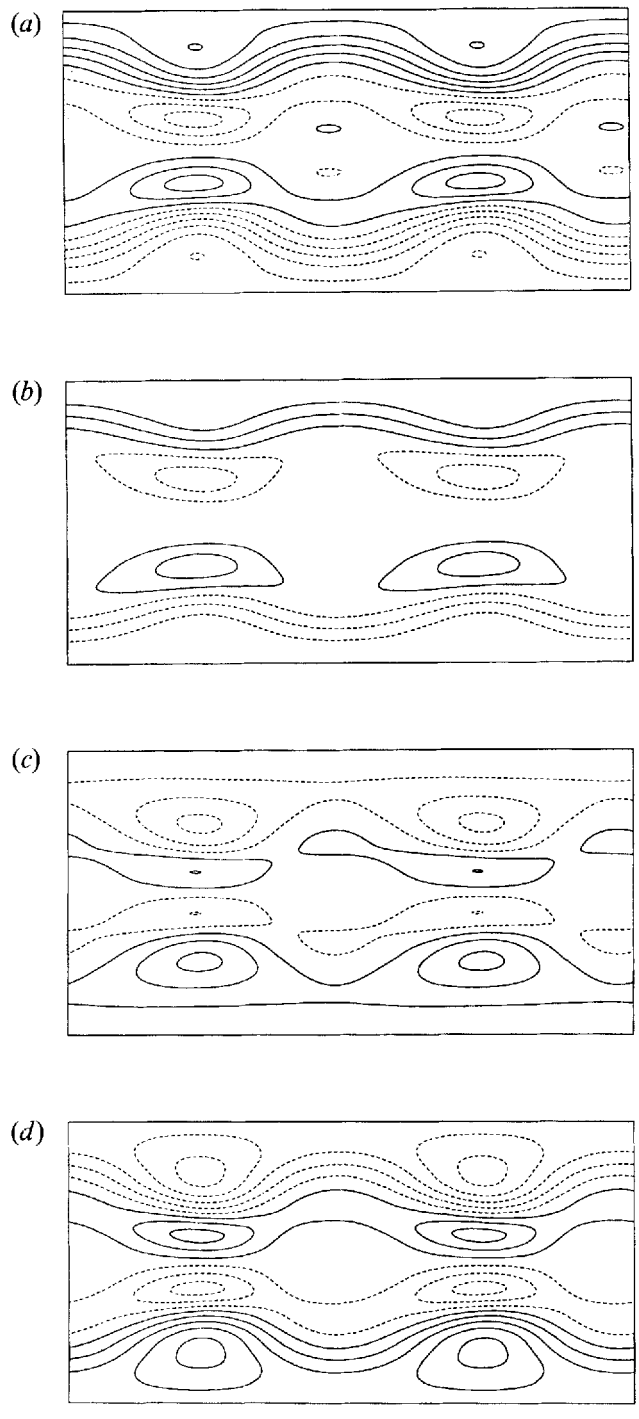

FIGURE 8. The radial magnetic field on $r = 1$ for the marginal oscillatory $E^4P_2^S$ solution B detailed in figure 5. (*a*)–(*d*) show B_r on $r = 1$ at $\omega t = 0$, $\pi/4$, $\pi/2$ and $3\pi/4$ respectively. Contours are from −7.25 to 7.25; other details are as for figure 4.

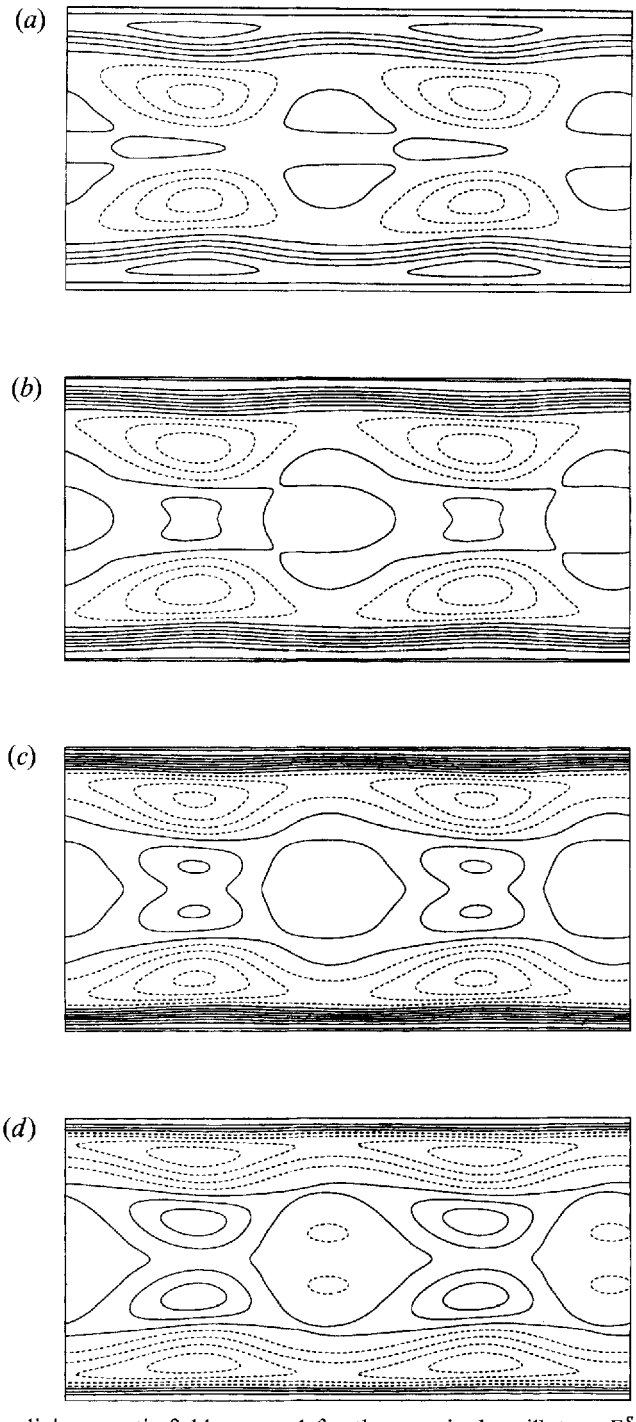

FIGURE 9. The radial magnetic field on $r = 1$ for the marginal oscillatory $E^S P_2^S$ solution F detailed in figure 6. (*a*)–(*d*) show B_r at $\omega t = 0$, $\pi/4$, $\pi/2$ and $3\pi/4$ respectively. Contours are from -25 to 50; other details are as for figure 4.

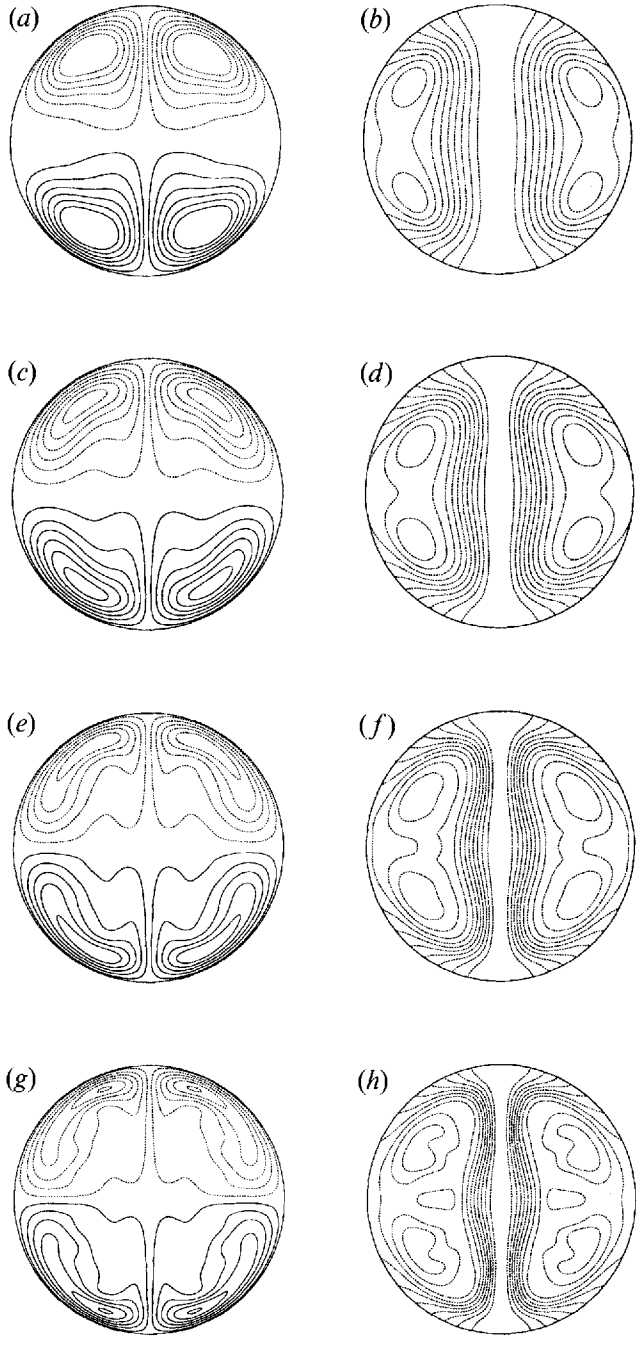

FIGURE 10. The axisymmetric field of stationary $E^A P_2^S$ solutions obtained for $p = 3\pi$, $\epsilon_2 = \epsilon_3 = 0.04$, with varying $\epsilon_1 > 0$, truncation level $(L, N) = (14, 150)$. (*a,b*) B_ϕ and F_ϕ for $\epsilon_1 = 0.01$, $R_m^c = 4604.41$. (*c,d*) B_ϕ, F_ϕ for $\epsilon_1 = 0.04$, $R_m^c = 3918.47$. (*e,f*) B_ϕ, F_ϕ for $\epsilon_1 = 0.08$, $R_m^c = 4669.93$. (*g,h*) B_ϕ, F_ϕ for $\epsilon_1 = 0.12$, $R_m^c = 5596.33$. Contours of B_ϕ are from -300 to 300, of F_ϕ from -1.5 to 0; other details are as for figure 4.

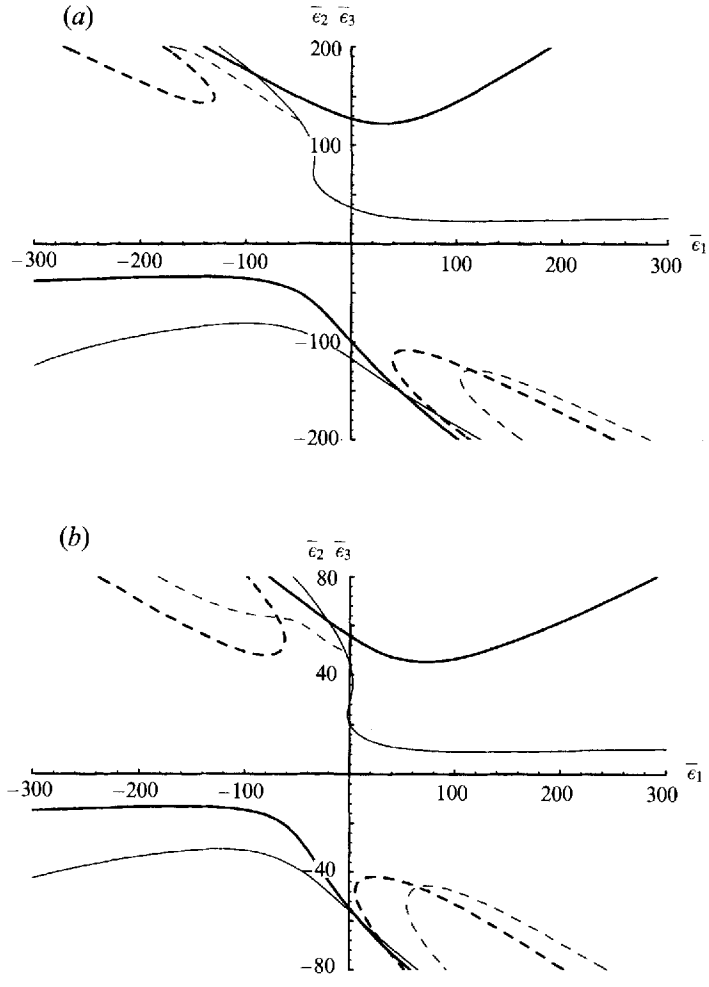

FIGURE 11. Critical stability curves, $\bar{\epsilon}_2\bar{\epsilon}_3$ with $\bar{\epsilon}_1$, for the Braginsky limit with (*a*) $p = \pi$, (*b*) $p = 2\pi$.

dynamo action, and dynamo efficiency greatest for $\epsilon_2 = \epsilon_3$; the imbalance in the two components of the convective cells present when $\epsilon_2 \neq \epsilon_3$ results in more energy being diverted to the non-axisymmetric magnetic field at the expense of the axisymmetric field whose maintenance, by the α-effect mechanism outlined by Braginsky, is necessary for dynamo action. Thus, comparing solutions with $\epsilon_2\epsilon_3 = 0.0016$, 98.90% of the magnetic energy (94.60% ohmic dissipation) is in the axisymmetric field for the case $(\epsilon_2, \epsilon_3) = (0.04, 0.04)$, in contrast with 97.09% (87.77%) and 97.49% (88.62%) for the cases $(\epsilon_2, \epsilon_3) = (0.02, 0.08)$ and $(0.08, 0.02)$ respectively. In the extreme cases of imbalance $\epsilon_2 \approx 0$ or $\epsilon_3 \approx 0$, dynamo action cannot be obtained, as could be anticipated from consideration of the asymptotic limit, where both $\sin m\phi$ and $\cos m\phi$ components must be present for a non-zero α-effect to be produced.

3.4. *Solutions of other symmetries*

For the KR velocity, the discussion of §2.2 showed that kinematic solutions of $E^S P_2^S$, $E^A P_2^S$, $E^S P_2^A$, and $E^A P_2^A$ morphologies all exist independently; solutions of each of these symmetries were therefore investigated. Figure 17 shows the growth rates of the least rapidly decaying modes as a function of R_m, for the KR velocity with $p = 3\pi$,

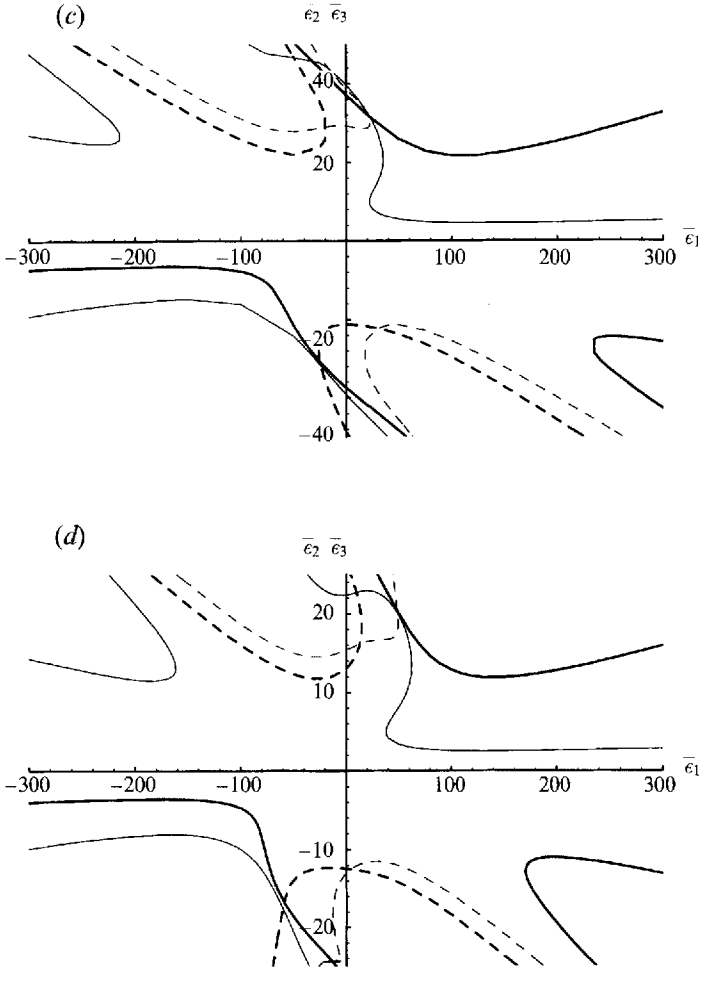

FIGURE 11. (*c*) $p = 3\pi$, (*d*) $p = 4\pi$, from calculations at $(L, N) = (14, 40)$. Line types are as for figure 1.

$\epsilon_1 = 0.03$, $\epsilon_2 = \epsilon_3 = 0.04$, at truncation level $(L, N) = (12, 100)$. The $E^A P_2^S$ solution KR investigated has $R_m^c \approx 3883$ at this truncation; none of the other symmetries achieve positive growth rates within this range of R_m, so that the $E^A P_2^S$ solution is indeed the most easily excited. The solutions whose eigenvalues have positive real part are here oscillatory for all symmetries other than $E^A P_2^S$.

Similar investigations for other velocity parameters confirm that the solution branches illustrated in the previous sections do represent the most easily excited modes, the $E^S P_2^S$ solution in many cases, detailed above, being the most easily excited. In all cases investigated, however, growth rates for the two P_2^A symmetries remain negative. This is perhaps not surprising, as these symmetries do not contain the axisymmetric components expected by Braginsky's analysis to dominate the high-R_m regime.

4. The adjoint symmetry and the influence of the boundary

4.1. *The adjoint symmetry*

In addition to allowing an investigation of the approximate symmetry between E^S and E^A eigenvalues of systems with velocities of opposite sense, observed above,

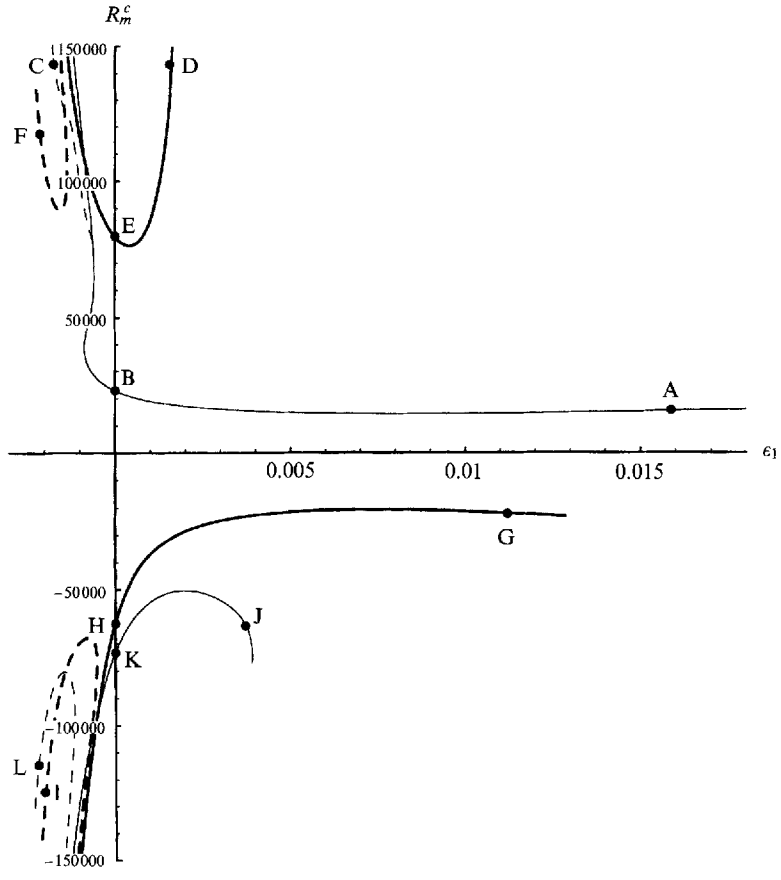

FIGURE 12. Predicted R_m^c variations for $\epsilon_2 = \epsilon_3 = 0.04$, from extrapolation of Braginsky limit results for $p = \pi$ at $(L, N) = (14, 40)$. Line types are as for figure 1. Points A–L are referred to in the text.

the adjoint systems introduced in §2.3 allow a straightforward yet non-trivial test of our numerical method. The interaction terms arising in (2.21)–(2.21) differ markedly between the physical E^A system and the adjoint E^S system, and so the required symmetry of eigenvalues can only be observed if all interactions are accurately represented numerically.

To investigate the adjoint of Kono & Roberts (1991), we need only invert the sign of all interaction terms in the induction equation. Table 5 shows the eigenvalues of the most easily excited solutions of the dynamo and adjoint systems, for the KR velocity with both $R_m > 0$ and $R_m < 0$. The symmetry of Richardson-extrapolated eigenvalues – between E^S adjoint solutions and E^A dynamo solutions, and vice versa – is satisfied to 4 significant figures, a satisfactory result. This table also highlights the approximate symmetry between physical E^A and E^S solutions noted previously; the deviation in $|R_m^c|$ between the E^A and E^S solutions of the dynamo systems with $R_m > 0$ and $R_m < 0$ is only of order 15 %, illustrating the finite influence of the boundary which motivates the investigations in §4.2.

Solutions for R_m^c could only be obtained for the P_2^S symmetries (the P_2^A symmetries permitting no growing solutions for this velocity, as detailed in §3.4). Growth-rate eigenvalues were investigated for all solution symmetries, however, and results are

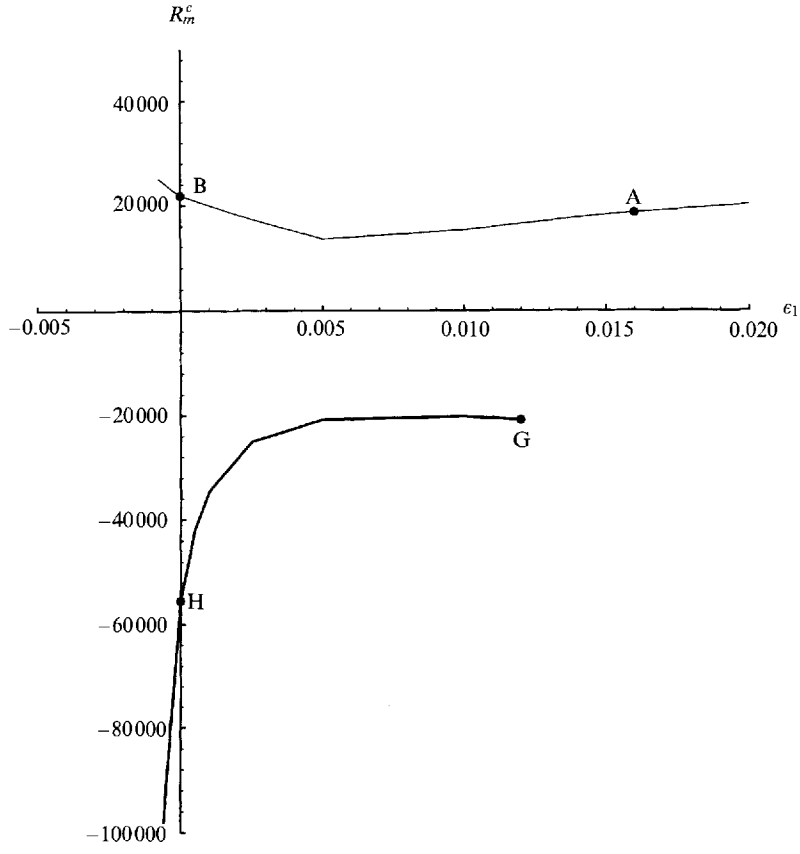

FIGURE 13. True R_m^c variation for $\epsilon_2 = \epsilon_3 = 0.04$, for $p = \pi$ at $(L, N) = (16, 150)$. The points marked refer to the corresponding solutions in figure 12; line types are as for figure 1.

given in table 6.† The agreement is once more reasonable, verifying that our numerical technique satisfactorily represents interactions for all these symmetries.

The $\alpha\omega$-code employed for Braginsky limit calculations was also verified through solution of the adjoint system; the adjoint symmetry is satisfactorily obtained, with results agreeing well with those given by Kono & Roberts (1991).

The comparison system of Proctor (1977*b*) allowed the adjoint symmetry between E^A and E^S modes under $\boldsymbol{u} \rightarrow -\boldsymbol{u}$ to be established. Although the boundary conditions invoked by Proctor are unphysical, they asymptotically approach the physical boundary conditions in the limit of thick conducting external shells, a limit investigated in the following. Therefore the comparison system, which also allows a further global check on our numerical method, is investigated numerically, through solving the induction equation with the boundary condition (2.12) imposed. Table 7 shows growth-rate eigenvalues obtained with this system for each solution symmetry of the KR velocity with $R_m = \pm 4000$. The agreement between E^A solutions for $R_m > 0$ and E^S solutions for $R_m < 0$, and vice versa, is excellent.

† In this and in subsequent tables, only Richardson extrapolated eigenvalues will be quoted, these being calculated as before. Full details of the calculations are avaliable from the authors or the JFM Editorial Office.

Point A: E^A, $\epsilon_1 = 0.016$ (Brag. limit $\Rightarrow$ 15600)

$L_\Delta \backslash N$	100	150	$O(h^4)$
14	17506.6	18613.9	19499.8
16	17512.6	18641.9	19545.4
18	18249.2	18273.1	18292.2
20	17518.2	18633.8	19526.2
22	17517.8	18631.5	19522.5
24	17517.9	18629.3	19518.4

Point B: E^A, $\epsilon_1 = 0$ (Brag. limit $\Rightarrow$ 22900)

$L_\Delta \backslash N$	100	150	$O(h^4)$
14	20112.2	21876.1	23287.3
16	20108.9	21871.5	23281.7
18	20108.1	21869.9	23279.3
20	20108.1	21869.7	23279.0
22	20108.1	21869.7	23279.0
24	20108.1	21869.7	23279.0

Point G: E^S, $\epsilon_1 = 0.012$ (Brag. limit $\Rightarrow -21900$)

$L_\Delta \backslash N$	100	150	$O(h^4)$
14	−20135.9	−21296.8	−22225.5
16	−20427.2	−21669.4	−22663.2
18	−20246.3	−21441.8	−22398.3
20	−20351.3	−21560.9	−22528.6
22	−21148.7	−21301.8	−21424.3
24	−20298.8	−21501.7	−22464.1

Point H: E^S, $\epsilon_1 = 0$ (Brag. limit $\Rightarrow -61900$)

$L_\Delta \backslash N$	100	150	$O(h^4)$
14	—	—	—
16	−48171.2	−56047.2	−62348.0
18	−48701.4	−55994.7	−61829.3
20	−48525.9	−55697.1	−61434.1
22	−48346.3	−55585.4	−61376.7
24	−48219.8	−55637.6	−61571.8

TABLE 3. Convergence of R_m^c eigenvalues of selected 3D solutions, $p = \pi$. The solutions chosen approximate the extrapolations of the Braginsky limit solutions given above for $\epsilon_2 = \epsilon_3 = 0.04$. (The eigenvalues anticipated from the extrapolation are given in the header captions.) The triangular truncation scheme was used for these calculations, with L_Δ up to 24.

4.2. *Dynamo systems with quiescent conducting external shells*

The preceding section verified the symmetry of eigenvalues pertaining to two different mutually adjoint systems, both involving unphysical boundary conditions. To relate these results to physical dynamo systems, we must link these solutions to solutions employing physically reasonable boundary conditions. This is done through consideration of dynamo systems with quiescent conducting shells external to the active dynamo region. Such layers have been incorporated into kinematic dynamo models by previous authors, including Bullard & Gubbins (1977), Serebrianya (1988) and Hutcheson & Gubbins (1994).

The altered boundary conditions obtained upon the addition of a shell of thickness $d - 1$ outside the fluid sphere $r < 1$, are given for both the physical and comparison systems in (2.13*a*)–(2.14); we have here specialized to the stationary case.

Eigenvalues for the dynamo and comparison systems with various d are given in table 8, with both E^A solutions ($R_m > 0$) and E^S solutions ($R_m < 0$) being considered.

E^A

$\epsilon_2\backslash\epsilon_3$	0.02	0.04	0.08	0.12	0.16
0.02	17380.1	7147.11	4209.65	3720.38	3846.38
0.04	8018.40	3892.82	2457.14	2135.74	2139.98
0.08	5839.15	2814.43	1654.82	1330.82	1234.19
0.12	6982.59	2917.20	1486.28	1084.60	926.802
0.16	11879.7	3752.17	1597.57	1025.72	798.450

E^S

$\epsilon_2\backslash\epsilon_3$	0.02	0.04	0.08	0.12	0.16
0.02	—	−9522.53	−5193.39	—	—
0.04	−8483.40	−4545.98	−3243.79	−2995.58	—
0.08	−4281.03	−3139.71	−2467.42	−2220.14	−2243.69
0.12	−3835.58	−3001.44	−2289.97	−1931.10	−1809.05
0.16	−3987.38	−3250.02	−2285.65	−1793.36	−1554.50

TABLE 4. R_m^c eigenvalues for selected values of ϵ_2 and ϵ_3, for the KR velocity with $p = 3\pi, \epsilon_1 = 0.03$, at truncation level $(L, N) = (12, 150)$.

		$\backslash N$	50	100	150	$O(h^6)$
$R_m > 0$	Dynamo	E^A	3832.80	3882.67	3892.80	3901.11
	Adjoint	E^S	4634.76	4055.27	3967.49	3901.67
$R_m < 0$	Dynamo	E^S	−4755.81	−4576.20	−4543.58	−4517.63
	Adjoint	E^A	−4800.67	−4580.64	−4545.17	−4517.99

TABLE 5. Most easily excited eigenvalues (R_m^c) of the dynamo and adjoint systems with the KR velocity $p = 3\pi$, $\epsilon_1 = 0.03$, $\epsilon_2 = \epsilon_3 = 0.04$, for both positive and negative R_m. Calculations employed truncation level $L = 16$.

	Dynamo	Adjoint
$P_2^S E^S$	−23.7628 + 12.7560 i	0.191576 + 0 i
$P_2^S E^A$	0.190940 + 0 i	−23.7627 + 12.7563 i
$P_2^A E^S$	−216.121 + 358.663 i	−240.505 + 358.398 i
$P_2^A E^A$	−240.507 + 358.397 i	−216.119 + 358.666 i

TABLE 6. Growth-rate eigenvalues of largest real part for all solution symmetries of the dynamo and adjoint systems with the KR velocity $p = 3\pi$, $\epsilon_1 = 0.03$, $\epsilon_2 = \epsilon_3 = 0.04$, and $R_m = 4000$. Calculations employed truncation level $L = 14$, and $O(h^6)$ Richardson extrapolation from the eigenvalues obtained for $N = 50$, 100 and 150.

	$R_m = 4000$	$R_m = -4000$
$P_2^S E^S$	−29.8860 + 17.3549 i	−19.7926 + 0 i
$P_2^S E^A$	−19.7929 + 0 i	−29.8860 + 17.3549 i
$P_2^A E^S$	−234.136 + 3779.59 i	−223.063 + 3760.89 i
$P_2^A E^A$	−223.064 + 3760.89 i	−234.136 + 3779.59 i

TABLE 7. Growth rate eigenvalues of largest real part for all solution symmetries of the comparison problem with the KR velocity $p = 3\pi$, $\epsilon_1 = 0.03$, $\epsilon_2 = \epsilon_3 = 0.04$, and with $|R_m| = 4000$. Calculations employed truncation level $L = 14$, and $O(h^6)$ Richardson extrapolation from the eigenvalues obtained for $N = 50$, 100 and 150.

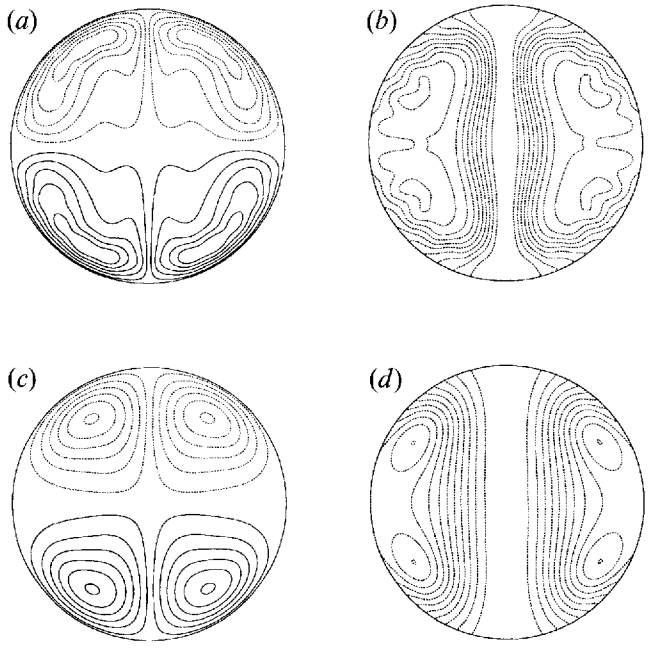

FIGURE 14. The axisymmetric field of the marginal stationary $E^A P_2^S$ solutions obtained for $p = \pi$, $\epsilon_2 = \epsilon_3 = 0.04$, $R_m > 0$, triangular truncation level $(L_A, N) = (24, 150)$. (*a*) B_ϕ, solution A with $\epsilon_1 = 0.016$, $R_m^c = 18629.3$, contours from -1.5 to 0. (*b*) F_ϕ, solution as for (*a*), contours from -1250 to 1250. (*c*) B_ϕ, solution B with $\epsilon_1 = 0$, $R_m^c = 21869.7$, contours from -1.25 to 0. (*d*) F_ϕ, solution as for (*c*), contours from -1750 to 1750. Other details are as for figure 4.

	Dynamo		Comparison	
d	E^A, $R_m > 0$	E^S, $R_m < 0$	E^A, $R_m > 0$	E^S, $R_m < 0$
1	3901.11	−4517.63	22473.6	−19754.6
1.0101	3611.60	−4269.01	15815.0	−16251.8
1.0526	2881.91	−3570.06	7408.71	−7414.60
1.1111	2418.47	−3038.56	4736.44	−4736.44
1.4286	1813.19	−2107.02	2315.27	−2315.25
2.5	1667.59	−1726.11	1735.09	−1735.08
10	1659.06	−1660.04	1660.06	−1660.05
∞	1659.05	−1659.04	1659.05	−1659.04

TABLE 8. Behaviour of R_m^c ($\omega = 0$) with varying d, for the KR velocity $p = 3\pi$, $\epsilon_1 = 0.03$, $\epsilon_2 = 0.04$, $\epsilon_3 = 0.04$. Solutions of both the dynamo and comparison systems are detailed; the convergence of the E^A eigenvalues for $R_m > 0$ and the E^S eigenvalues for $R_m < 0$, as $d \to \infty$, is shown for each system, as is the convergence of the two systems themselves in the same limit. Calculations employed truncation level $L = 16$, and $O(h^6)$ Richardson extrapolation from the eigenvalues obtained for $N = 50$, 100 and 150.

As required from the $d \gg 1$ limit (2.15), the physical and comparison system solutions converge towards each other as d increases; thus the physical E^A and E^S solutions for opposite senses of velocity tend towards equal $|R_m^c|$.

The values of R_m^c obtained for the physical cases $d = 1$ and $d = \infty$ differ by a factor of approximately 2.5, and so the insulating boundary clearly exerts a considerable influence on dynamo action. Nevertheless the boundary appears to influence E^A and E^S solutions approximately equally. Figure 18, which shows the axisymmetric fields

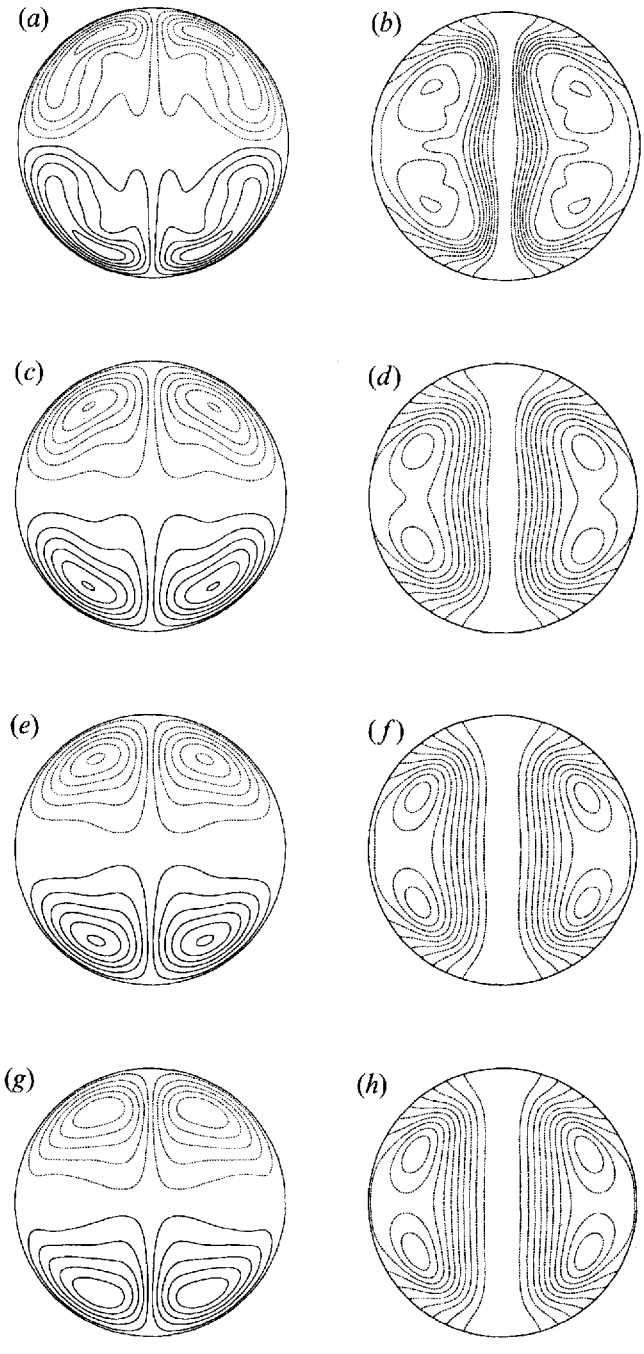

FIGURE 15. The axisymmetric field of the marginal stationary $E^A P_2^S$ solutions obtained for $p = 3\pi$, $\epsilon_1 = 0.03$ with varying $\epsilon_2 = \epsilon_3$, truncation level $(L, N) = (12, 150)$. (*a*) B_ϕ for $\epsilon_2 = \epsilon_3 = 0.02$, $R_m^c = 17380.1$, contours from -1.5 to 0. (*b*) F_ϕ, solution as for (*a*), contours from -1000 to 1000. (*c*) B_ϕ, for $\epsilon_2 = \epsilon_3 = 0.04$, $R_m^c = 3892.82$, contours from -1.5 to 0. (*d*) F_ϕ, solution as for (*c*), contours from -350 to 350. (*e*) B_ϕ for $\epsilon_2 = \epsilon_3 = 0.08$, $R_m^c = 1654.82$, contours from -1.5 to 0. (*f*) F_ϕ, solution as for (*e*), contours from -150 to 150. (*g*) B_ϕ for $\epsilon_2 = \epsilon_3 = 0.16$, $R_m^c = 798.450$, contours from -1.5 to 0. (*h*) F_ϕ, solution as for (*g*), contours from -65 to 65. Other details are as for figure 4.

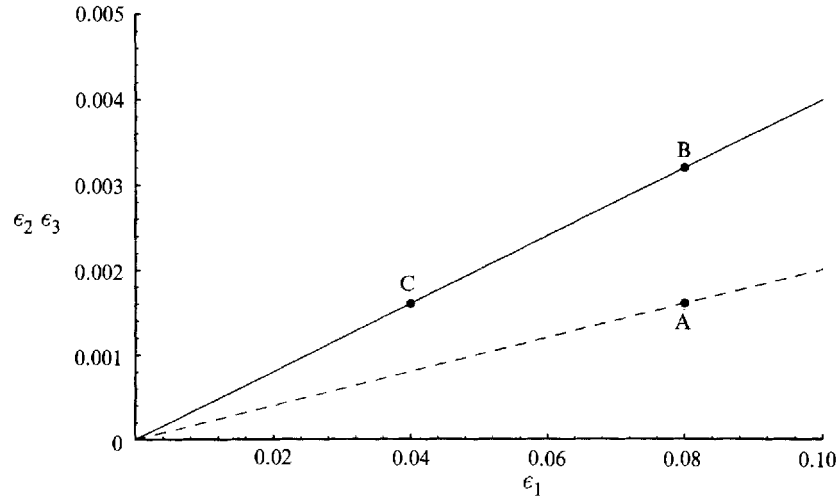

FIGURE 16. Relation between solutions with different $\epsilon_1/\epsilon_2\epsilon_3$. Two lines show the families of solutions with $\epsilon_1/\epsilon_2\epsilon_3 = 50$ (lower line) and $\epsilon_1/\epsilon_2\epsilon_3 = 25$ (upper line); distance from the origin along each line corresponds to deviation from the Braginsky limit. From point A, with $\epsilon_1/\epsilon_2\epsilon_3 = 50$, one can move to a solution with $\epsilon_1/\epsilon_2\epsilon_3 = 25$ either by increasing $\epsilon_2\epsilon_3$ (to point B) or by decreasing ϵ_1 (point C). Both B and C, lying on the same line, share a similar morphology, although the relative strength of their toroidal to poloidal, and axisymmetric to non-axisymmetric, components differ.

obtained for varying d, also shows that the solution morphology is not changed beyond recognition. In these two senses then, the boundary condition plays only a secondary role in determining the solutions of the dynamo system, allowing the approximate eigenvalue symmetry previously observed to be traced to the adjoint symmetries elucidated in §2.3.

For $d > 1$, the field morphology is considerably simpler, as toroidal flux is free to diffuse outside the sphere $r \leqslant 1$, resulting in lower diffusion, lower R_m^c, and correspondingly improved numerical convergence. The conclusion of Hutcheson & Gubbins (1994), that the presence of a quiescent conducting layer facilitates dynamo action, is thus upheld and extended to E^S solutions.

For the comparison problem the artificial $S = 0$ boundary condition compounds difficulties of dynamo action at low d, producing convoluted field and high R_m^c. The resultant poor numerical convergence is evident in the deviations from equality of E^A and E^S eigenvalues at the smaller values of d in table 8. A relatively small quiescent layer can significantly decrease these difficulties, however; for $d = 10/9$, R_m^c is significantly smaller, convergence reasonable, and the correspondence between E^A and E^S eigenvalues good. For slightly greater d (e.g. $d = 10/7$), the comparison problem proves a passable approximation to the dynamo problem, a result that may prove useful for future analytic work. For future numerical work we may also note that any method that concentrates the radial representation near the external boundary would also help overcome these numerical difficulties.

The deviations between dynamo and comparison systems can be investigated more quantitatively. Proctor (1977*b*) showed that the difference in eigenvalues must vary as $O(d^{-(2l+1)})$, where l is the lowest degree of poloidal field present. Thus the $E^A P_2^S$ solution should produce an $O(d^{-3})$ change in eigenvalues; an $E^S P_2^S$ solution, an $O(d^{-5})$ deviation. Figure 19 plots the differences between dynamo and comparison eigenvalues obtained numerically at high d along with the best-fitting curves of form

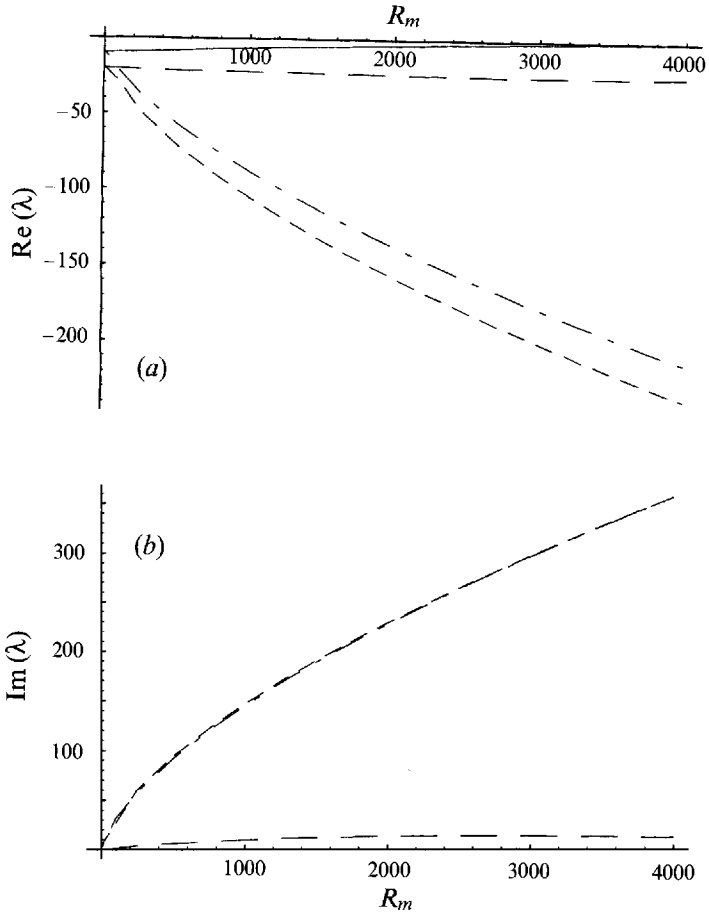

FIGURE 17. Growth rates, λ, of greatest real part with increasing R_m, for each symmetry of solution obtained for $p = 3\pi$, $\epsilon_1 = 0.03$, $\epsilon_2 = \epsilon_3 = 0.04$. Re λ is shown in (a), Im λ (the frequency, ω) in (b). The solid line shows the $E^A P_2^S$ solution, the long-dashed the $E^S P_2^S$, the short-dashed the $E^A P_2^A$, the chain-dashed the $E^S P_2^A$. (The $E^A P_2^S$ solution is stationary ($\omega = 0$).)

$O(d^{-3})$ (E^A) and $O(d^{-5})$ (E^S solutions); the excellent fit of the data to the curves confirms the well-behaved nature of the problem in the $d \gg 1$ limit.

4.3. *Dynamo systems with inner cores*

The preceding section considered the importance of the outer boundary on dynamo action, motivated by the adjoint symmetry anticipated in the limit $d \to \infty$; an inner boundary is also of potential import to planetary dynamos, and so is here investigated.

An inner core, of radius $b < 1$, may easily be incorporated into our model, simply by rescaling the velocity into the outer region of the sphere and dealing appropriately with the new internal boundary. For a conducting core, whose conductivity we take for simplicity to equal that of fluid region, we may in fact neglect the boundary magnetically, and continue to explicitly solve for $\boldsymbol{B}$ throughout $r < 1$. Alternatively, for stationary solutions, calculations similar to those used for the conducting quiescent layer produce the condition

$$\frac{\mathrm{d}T_l^m}{\mathrm{d}r} - \frac{l+1}{r} = 0, \qquad \frac{\mathrm{d}S_l^m}{\mathrm{d}r} - \frac{l+1}{r} S_l^m = 0, \qquad r = b. \tag{4.1}$$

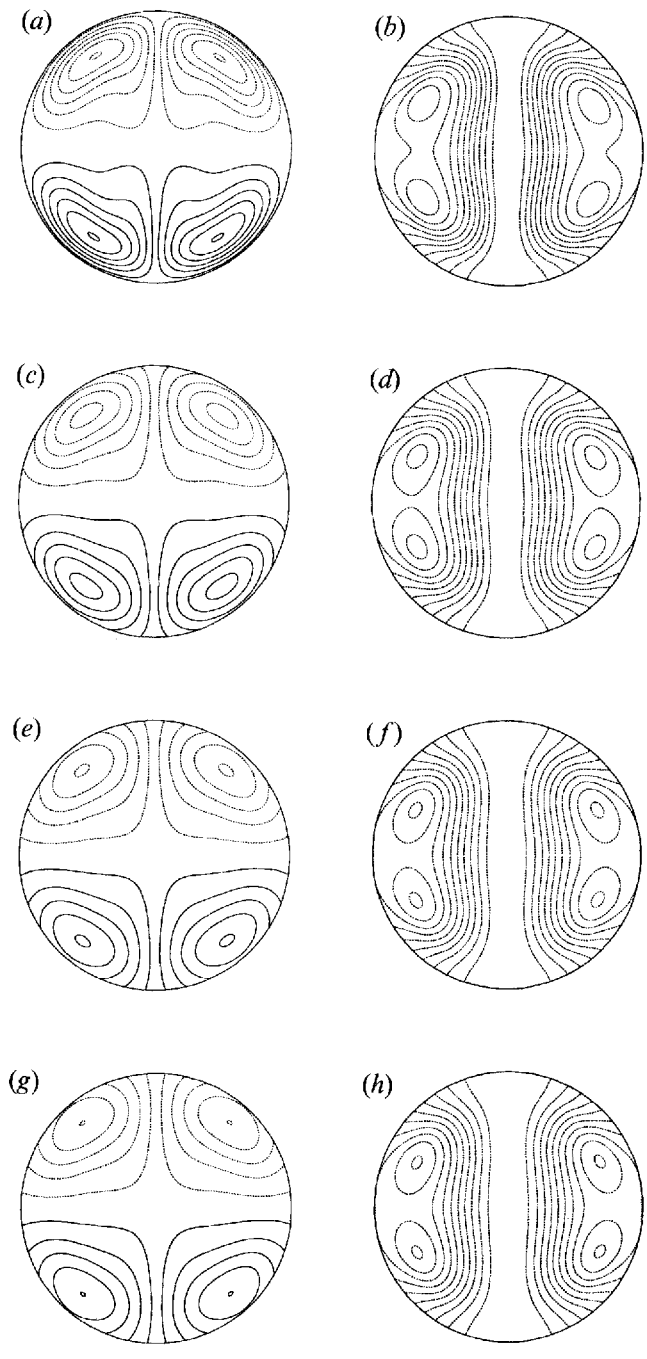

FIGURE 18. The axisymmetric field of the marginal $E^A P_2^S$ solutions obtained for $p = 3\pi$, $\epsilon_1 = 0.03$, $\epsilon_2 = \epsilon_3 = 0.04$, with varying d at $(L, N) = (16, 150)$. (*a,b*) B_ϕ and F_ϕ for $d = 1$, $R_m^c = 3892.8$. (*c,d*) B_ϕ, F_ϕ for $d = 10/9$, $R_m^c = 2417.9$. (*e,f*) B_ϕ, F_ϕ for $d = 10/7$, $R_m^c = 1813.3$. (*g,h*) B_ϕ, F_ϕ for $d = \infty$, $R_m^c = 1659.0$. Contours of B_ϕ are from -350 to 350, of F_ϕ from -1.5 to 0; other plot details are as for figure 4.

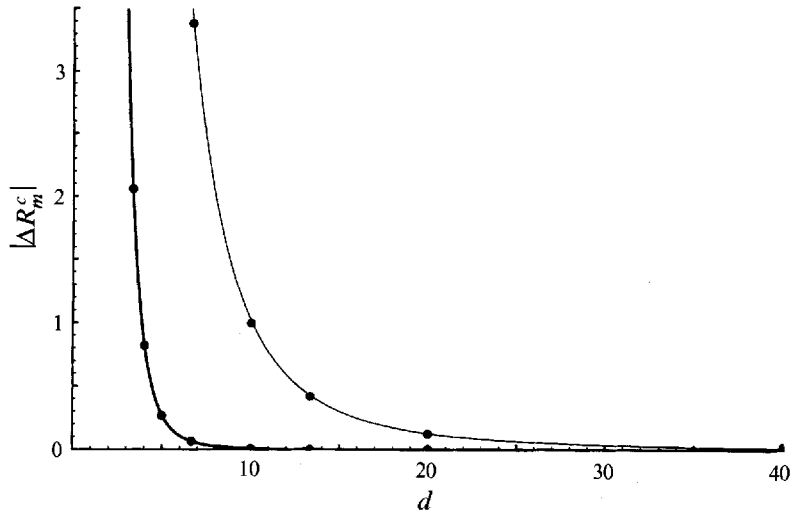

FIGURE 19. Differences in R_m^c between the dynamo and comparison systems, for E^A and E^S solutions, with the best-fitting $O(d^{-3})(E^A)$ and $O(d^{-5})(E^S)$ curves, for $p = 3\pi$, $\epsilon_1 = 0.03$, $\epsilon_2 = \epsilon_3 = 0.04$. E^A (E^S) solutions are shown by thin (thick) lines.

For an insulating core, the correct condition is

$$T_l^m = 0, \qquad \frac{\mathrm{d}S_l^m}{\mathrm{d}r} - \frac{l+1}{r} S_l^m = 0, \qquad r = b. \tag{4.2}$$

(Although an insulating core is of less obvious planetary relevance, it is of interest in light of the conclusions of Hollerbach & Jones (1993*a*), who found that the dynamical behaviour of a (conducting) core led to the internal expulsion of toroidal flux, a situation better modelled kinematically by an insulator than a conductor. The effect of the core's conductivity on dynamo action is also of interest given that previous authors (e.g. Zhang & Busse 1989) have for numerical simplicity employed insulating cores.)

The effect of a conducting core on the E^A and E^S solutions located above is given in table 9. If the values of R_m^c are rescaled to the new length scale, $\mathscr{L} = 1-b$, appropriate to the active dynamo region, it can be argued that cores of quite considerable size influence dynamo action only slightly. Thus, for $b \leqslant 0.5$, say, the change in dynamo efficiency can largely be explained by the simple reduction in the size of the effective dynamo region. The morphology of the field varies considerably over this range, however, as can be seen from figure 20; even a small inner core significantly modifies the flux in the interior, where the field can now only penetrate by diffusion. The variation in toroidal field is particularly noticeable. The resultant new flux features become more marked as b increases; in the present case they dominate the solution for $b \geqslant 0.5$, the original flux-pattern being overwhelmed. Beyond this point, the behaviour becomes more convoluted. It is clear that the solution is then to a large extent constrained by the imposed geometry.

Although the internal morphology can thus be seen to vary considerably, the externally visible field changes only slightly, as is seen, for the E^A solution, from figure 21.

For the KR velocity under investigation, the E^S solution morphology adapts more easily to the presence of the inner core than does the E^A; thus for values of b of approximately 0.3 or greater, the E^S solution possesses the smaller $|R_m^c|$. Thus it is

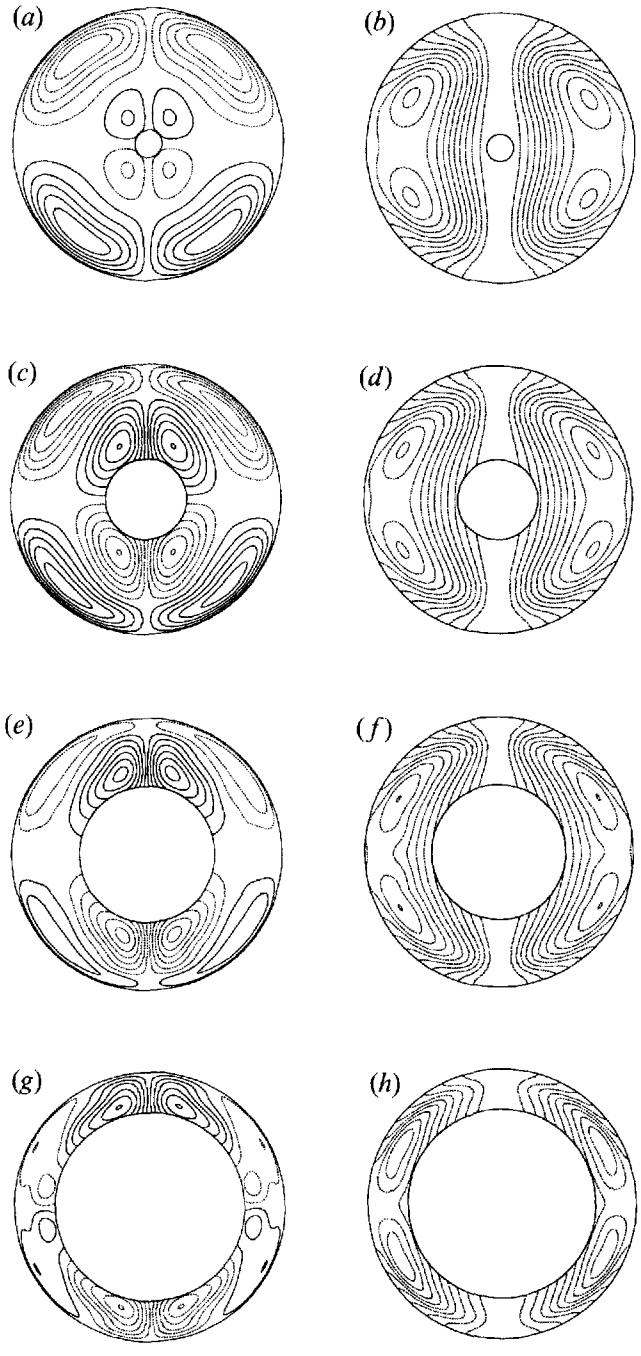

FIGURE 20. The axisymmetric field of the marginal $E^A P_2^S$ solutions obtained for $p = 3\pi$, $\epsilon_1 = 0.03$, $\epsilon_2 = \epsilon_3 = 0.04$, with varying conducting b, at $(L, N) = (16, 151)$. (*a*) B_ϕ for $b = 0.1$, $R_m^c = 4409.5$, contours from -1.4 to 0. (*b*) F_ϕ, solution as for (*a*), contours from -265 to 265. (*c*) B_ϕ for $b = 0.3$, $R_m^c = 5986.8$, contours from -1.35 to 0. (*d*) F_ϕ, solution as for (*c*), contours from -155 to 155. (*e*) B_ϕ for $b = 0.5$, $R_m^c = 8213.7$, contours from -1.3 to 0. (*f*) F_ϕ, solution as for (*e*), contours from -180 to 180. (*g*) B_ϕ for $b = 0.7$, $R_m^c = 8723.5$, contours from -1.7 to 0. (*h*) F_ϕ, solution as for (g), contours from -200 to 200. Other details are as for figure 4.

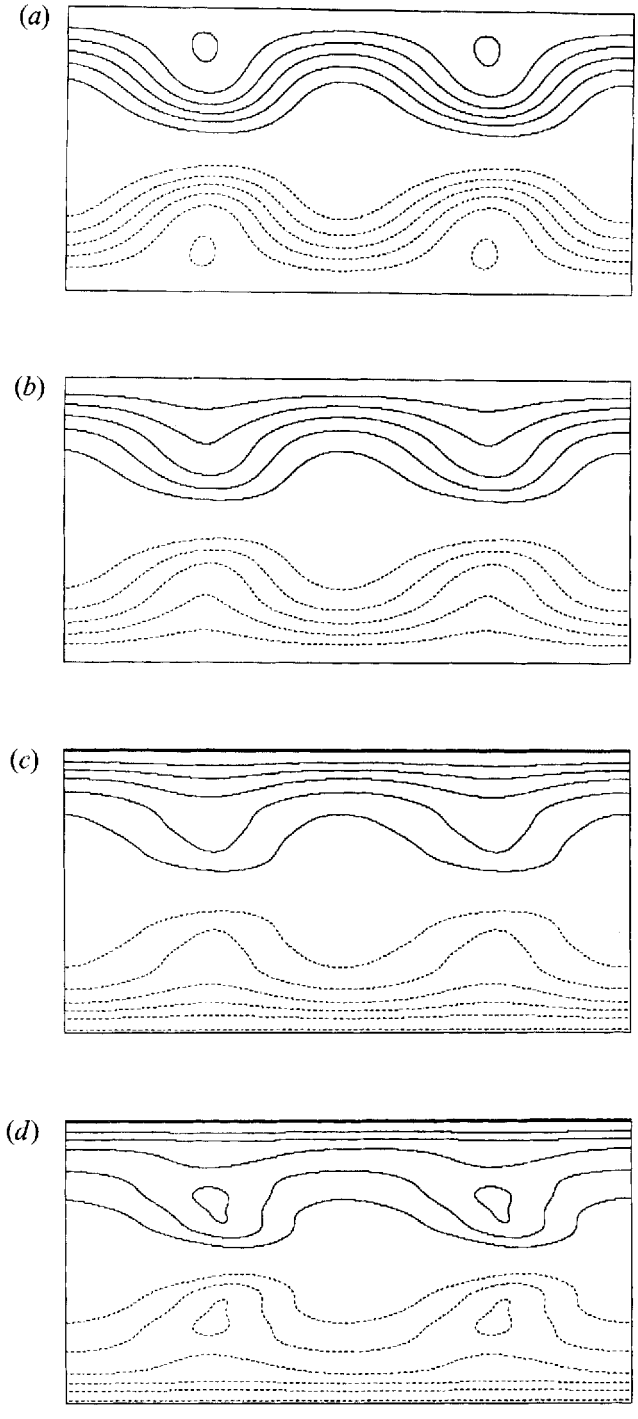

FIGURE 21. The radial field on $r = 1$ for the marginal $E^A P_2^S$ solutions obtained for $p = 3\pi$, $\epsilon_1 = 0.03$, $\epsilon_2 = \epsilon_3 = 0.04$, with varying conducting b, at $(L, N) = (16, 151)$. (*a*) B_r for $b = 0.1$, $R_m^c = 4449.1$, contours from -3.35 to 3.35. (*b*) B_r for $b = 0.3$, $R_m^c = 5986.8$, contours from -4.35 to 4.35. (*c*) B_r for $b = 0.5$, $R_m^c = 8213.7$, contours from -6.35 to 6.35. (*d*) B_r for $b = 0.7$, $R_m^c = 8723.5$, contours from -5.45 to 5.45. Other details are as for figure 4.

	Conducting		Insulating	
b	E^A	E^S	E^A	E^S
0.0	3901.11	−4517.63	3901.11	−4517.63
0.1	4463.35	−5116.21	4462.65	−5106.33
0.2	5153.01	−5747.50	5138.83	−5670.83
0.3	6014.52	−6290.37	5939.85	−6092.55
0.4	7008.09	−6367.43	6794.86	−6199.73
0.5	8234.97	−6534.55	7821.45	−6470.34
0.6	8796.70	−6691.97	8470.81	−7032.71
0.7	8721.10	−7494.48	8824.30	−9056.34

TABLE 9. R_m^c for E^A and E^S solutions for the KR velocity $p = 3\pi$, $\epsilon_1 = 0.03$, $\epsilon_2 = \epsilon_3 = 0.04$ with varying inner cores b. Both conducting and insulating inner cores are detailed. Calculations employed truncation level $L = 16$, and $O(h^6)$ Richardson extrapolation from the eigenvalues obtained for $N = 51$, 101 and 151.

not inconceivable that a small inner core such as that in the Earth (where $b \approx 0.35$) may play a role in parity selection, although it must be remembered that the sign of R_m will be imposed by the hydrodynamics.

Critical eigenvalues for the KR solutions with an insulating core are also given in table 9, for comparison with the values obtained with a conducting core. It can be seen that the eigenvalues for the two cases differ only slightly, with the solutions for conducting cores being marginally more easily excited for all but the largest b. The field morphology changes almost negligibly; the toroidal field is now excluded from the inner core, but adapts to this constraint with relative ease.

Thus the effect of an insulating medium in the core can be seen, at least kinematically, to be slight. This fact might in future be employed to simplify the work involved in solving for time-dependent solutions, the insulating core allowing a simple matching condition to be adopted, removing the need for a numerical solution in the interior.

Although time-dependent fields might be expected to be more influenced by a core than the stationary solutions considered here – since a frequency-dependent skin-depth effect may exacerbate the exclusion of flux from the inner core – the similar nature of solutions obtained with conducting and insulating cores for oscillatory solutions obtained for an axisymmetric flow (Sarson 1994), show that this skin-depth effect need not be dominant. Its importance may also be to some extent decreased dynamically, when the inner core will be free to co-rotate with the magnetic field, a situation considered by Hollerbach & Jones (1993*a*, *b*).

5. Conclusions

The preceding calculations have succeeded in obtaining dynamo action, and agree well with the conclusions of previous authors in favouring the production of a stationary dipolar ($P_2^S E^A$) field for certain values of the velocity parameters. The surface field morphology obtained, essential for relating studies to the geodynamo, as considered in Gubbins & Sarson (1994), allows promising comparisons with the observed magnetic field, and can to some extent be understood in terms of simple flux advection mechanisms. In addition, however, many new solutions, of varying spatial and time symmetries have been obtained – in particular the $P_2^S E^S$ and the oscillatory P_2^S solutions are, we believe, the first of their kind – thus allowing a greater

understanding of the possibilities of dynamo action, and giving greater constraints on the flow responsible for the geodynamo.

The principal factor controlling the preference of the 3D system to stationary or oscillatory instabilities is the meridional circulation, as was also the case for the $\alpha\omega$-systems investigated by Roberts (1972). For the 3D systems, however, it is the effective meridional circulation arising in the asymptotic theory of Braginskiĭ (1964*a*), incorporating the azimuthal average of the non-axisymmetric velocity, that is important. In the past this feature of the theory appears to have been considered simply as a mathematical artifice and consequently neglected. The calculations detailed here confirm the validity and importance of this effect; its omission in the $\alpha\omega$-parameterization would lead to misleading results.

In so-called 'intermediate' dynamo models, where the dynamics under simple imposed α- and ω-effects are investigated, previous workers have employed rather particular distributions of α (e.g. Braginsky 1978; Braginsky & Roberts 1987), or a perhaps inappropriate reinstatement of the α^2 mechanism (e.g. Barenghi 1993; Hollerbach, Barenghi & Jones 1993), to ensure that the stationary solutions appropriate to modelling the geodynamo are obtained. The effective meridional circulation highlighted here is however of exactly the form required for this. This term, which emerges naturally from the asymptotic theory, may be prescribed with as much justification as the α-effect, and it would be more satisfactory to prescribe a non-axisymmetric velocity explicitly, and calculate both the α-effect and the effective meridional circulation from this using the asymptotic prescriptions.

The preference of the 3D system for instabilities of dipole or quadrupole (E^A or E^S) symmetry is determined by the sense of the velocity, as previously observed for $\alpha\omega$-models (e.g. Kono & Roberts 1991); if $\boldsymbol{u}$ favours an E^S instability, $-\boldsymbol{u}$ will favour an E^A one. As the momentum equation in the presence of Coriolis and buoyancy forces is clearly not invariant under $\boldsymbol{u} \rightarrow -\boldsymbol{u}$, the symmetry type preferred will thus be determined by the governing dynamics. For non-axisymmetric velocity components of a given azimuthal wavenumber, the operation $\boldsymbol{u} \rightarrow -\boldsymbol{u}$ can, as pointed out by Proctor (1977*b*), be simply related to a rotation of the coordinate system in ϕ, an operation under which the system must be invariant; it is therefore the sense of the mean circulation, and in particular the dominant differential rotation, that will in practice determine the symmetry of solution preferentially excited.

Through variations in the outer boundary condition imposed, the influence of the sense of $\boldsymbol{u}$ on the preferred instability symmetry could be traced to the adjoint systems introduced in §2.3. The presence of the insulating boundary, whilst destroying the exact symmetry between E^A and E^S solutions observed under $\boldsymbol{u} \rightarrow -\boldsymbol{u}$, does not, at least for this velocity, influence the parity selection. Confirming the conclusions of Bullard & Gubbins (1977) and Hutcheson & Gubbins (1994), however, it does increase the ohmic dissipation produced, making dynamos harder to excite and increasing problems of numerical convergence.

The presence of an inner boundary, either conducting or insulating, had by comparison a relatively slight effect on the ease of dynamo action, at least until the size of the imposed inner core altered the geometry of the problem beyond recognition. Such an inner core may be expected to play a considerably greater role dynamically, however, as recent calculations (Hollerbach & Jones 1995, and references therein) show that a correctly coupled conducting inner core can completely change the nature of solutions obtained, since the absence of advection in the interior allows the magnetic field there to change only on the longer diffusion time scale, thus stabilizing the system.

No positive dynamo action could be obtained for the P_2^A symmetries, for any values of the velocity parameters investigated. This was to be expected in the Braginsky regime, where velocities approaching the nearly axisymmetric asymptote were considered. Such solutions are, however, to be expected in another regime, with flows characterized by $\epsilon_2 \approx \epsilon_3 \approx 0$, $\epsilon_1 \sim O(1)$, closely related to the $t_1^0 s_2^0$ flow found by Dudley & James (1989) to produce equatorial dipole fields. A brief investigation of the KR velocity in this regime did not locate dynamo action (Sarson 1994). These investigations were hampered by the numerical resolutions attainable, however, and this conclusion may prove a numerical artefact.

Numerical convergence remains a problem in investigations of dynamo action. Cases were obtained where dynamo action appeared to occur at low truncations but later proved to be spurious; in other instances low truncations were unable to adequately represent a dynamo solution that finer resolution uncovered; in further situations the limited numerical resolution attainable was insufficient to allow us to investigate values of R_m high enough to obtain dynamo action with certainty. For investigations in the Braginsky regime, however, a convincing agreement between the 3D solution and the corresponding asymptotic approximation provides an invaluable test on numerical convergence. In addition, the adjoint systems investigated allow a further useful test that solutions are being adequately represented at finite truncation levels.

A degree of spatial complexity in the flow, previously thought to be essential for dynamo action (e.g. KR), appears not to be critical, flows with a simple single-cell structure in radius being capable of producing growing magnetic fields. A certain radial complexity assists dynamo action, however, resulting in a smaller R_m^c and better numerical convergence. Thus it aids numerical investigations in the same way that a non-insulating boundary layer does.

In relating our results to the geodynamo, we conclude that the predominantly stationary nature of the observed field can be explained with reference to the effective meridional circulation of the fluid flow in the core. The dependence of this feature on the strength of the non-axisymmetric convection (via $\epsilon_2\epsilon_3$ in our simple model) allows variations in the time behaviour of the geodynamo to be explained simply in terms of fluctuations in the convective strength, rather than requiring hypothetical shifts in the latitude of dominant convection, as Parker (1969) and Levy (1972) propose.

We may also conclude that the observed dipole nature of the field must be explained with reference to the sense of the differential rotation. More dynamical work needs to be done on the mechanisms producing this component of flow, to allow further insight into the MHD processes occurring in the core.

We thank Dr N. Barber for help with the calculations. This work was supported by NERC grant GR3/8238. During the course of the work, G.R.S. was supported by a NERC research studentship; whilst preparing this article, he benefited from a grant from the EC 'Nonlinear Phenomena and Complex Systems' network, and the hospitality of Professor F. H. Busse and the Universität Bayreuth.

REFERENCES

ABRAMOWITZ, M. & STEGUN, I. A. 1965 *Handbook of Mathematical Functions*. Dover.

BACKUS, G. E. 1958 A class of self-sustaining dissipative spherical dynamos. *Ann. Phys.* **4**, 372–447.

BARENGHI, C. F. 1993 Nonlinear planetary dynamos in a rotating spherical shell: III $\alpha^2\omega$ models and the geodynamo. *Geophys. Astrophys. Fluid Dyn.* **71**, 163–185.

BRAGINSKIĬ, S. I. 1964*a* Self-excitation of a magnetic field during the motion of a highly conducting fluid. *Zh. Eksp. Teor. Fiz.* **47**, 1084. English translation, *Sov. Phys. JETP* **20**, 726–735, 1965.

BRAGINSKIĬ, S. I. 1964*b* Theory of the hydromagnetic dynamo. *Zh. Eksp. teor. Fiz.* **47**, 2178 (English translation, *Sov. Phys. JETP* **20**, 1462–1471, 1965).

BRAGINSKY, S. I. 1978 Nearly axially symmetric models of the hydromagnetic dynamo of the Earth II. *Geomag. Aeron.* **18**, 225–231.

BRAGINSKY, S. I. & ROBERTS, P. H. 1987 A model-Z geodynamo. *Geophys. Astrophys. Fluid Dyn.* **38**, 327–349.

BULLARD, E. C. & GELLMAN, H. 1954 Homogeneous dynamos and terrestrial magnetism. *Proc. R. Soc. Lond.* A **247**, 213–278.

BULLARD, E. C. & GUBBINS, D. 1977 Generation of magnetic fields by fluid motions of a global scale. *Geophys. Astrophys. Fluid Dyn.* **8**, 43–56.

CONTE, S. D. 1966 The numerical solution of linear boundary value problems. *SIAM Rev.* **8**, 309–321.

DUDLEY, M. L. & JAMES, R. W. 1989 Time dependent dynamos with stationary flows. *Proc. R. Soc. Lond.* A **425**, 407–429.

GIBSON, R. D. & ROBERTS, P. H. 1966 Some comments on the theory of homogeneous dynamos. In *Magnetism and the Cosmos* (ed. W. Hindmarsh, F. H. Lowes, P. H. Roberts & S. K. Runcorn), pp. 108-120. Oliver and Boyd.

GUBBINS, D. 1972 Kinematic dynamos and geomagnetism. *Nature* **238** PS, 119–121.

GUBBINS, D. 1973 Numerical solutions of the kinematic dynamo problem. *Phil. Trans. R. Soc. Lond.* A **274**, 493–521.

GUBBINS, D. 1993 Geomagnetism and inferences for core motion. In *Flow and Creep in the Solar System: Observations, Modelling and Theory* (ed. D. B. Stone & S. K. Runcorn), pp. 97–111. Kluwer Academic.

GUBBINS D., MASTERS, T. G. & JACOBS, J. A. 1979 Thermal evolution of the Earth's core. *Geophys. J. R. Astron. Soc.* **59**, 57–99.

GUBBINS, D. & SARSON, G. 1994 Geomagnetic field morphology and kinematic dynamos. *Nature* **368**, 51–55.

GUBBINS, D. & ZHANG, K. 1993 Symmetry properties of the dynamo equations for paleomagnetism and geomagnetism. *Phys. Earth Planet. Inter.* **75**, 225–241.

HERZENBERG, A. & LOWES, F. J. 1957 Electromagnetic induction in rotating conductors. *Phil. Trans. R. Soc. Lond.* A **249**, 507–584.

HIDE, R. & PALMER, T. N. 1982 Generalisation of Cowling's theorem. *Geophys. Astrophys. Fluid Dyn.* **19**, 301–309.

HOLLERBACH, R., BARENGHI, C. F. & JONES, C. A. 1993 Taylor's constraint in a spherical $\alpha\omega$-dynamo. *Geophys. Astrophys. Fluid Dyn.* **67**, 3–25.

HOLLERBACH, R. & JONES, C. A. 1993*a* A geodynamo model incorporating a finitely conducting inner core. *Phys. Earth Planet. Inter.* **75**, 317–327.

HOLLERBACH, R. & JONES, C. A. 1993*b* Influence of the Earth's inner core on geomagnetic fluctuations and reversals. *Nature* **365**, 541–543.

HOLLERBACH, R. & JONES, C. A. 1995 On the magnetically stabilising role of the Earth's inner core. *Phys. Earth Planet. Inter.* **87**, 171–181.

HUTCHESON, K. A. 1990 Geomagnetic field modelling. PhD thesis, University of Cambridge.

HUTCHESON, K. A. & GUBBINS, D. 1994 Kinematic magnetic field morphology at the core mantle boundary. *Geophys. J. Intl* **116**, 304–320.

KONO, M. & ROBERTS, P. H. 1991 Small amplitude solutions of the dynamo problem: 1. The adjoint system and its solutions. *J. Geomagn. Geoelectr.* **43**, 839–862.

KRAUSE, F. & RÄDLER, K.-H. 1980 *Mean Field Magnetohydrodynamics and Dynamo Theory.* Akademie.

KUMAR, S. & ROBERTS, P. H. 1975 A three-dimensional kinematic dynamo. *Proc. R. Soc. Lond.* A **344**, 235–238 (referred to herein as KR).

LEVY, E. H. 1972 On the state of the geomagnetic field and its reversals. *Astrophys. J.* **175**, 573–581.

LILLEY, F. E. M. 1970 On kinematic dynamos. *Proc. R. Soc. Lond.* A **316**, 153–167.

MELCHIOR, P. 1986 *The Physics of the Earth's Core — An Introduction.* Pergamon.

MOFFATT, H. K. 1978 *Magnetic Field Generation in Electrically Conducting Fluids.* Cambridge University Press.

NAKAJIMA, T. & KONO, M. 1991 Kinematic dynamos associated with large scale fluid motions. *Geophys. Astrophys. Fluid Dyn.* **60**, 177–209.

PARKER, E. N. 1969 The occasional reversal of the geomagnetic field. *Astrophys. J.* **158**, 815–827.

PARKER, E. N. 1979 *Cosmical Magnetic Fields: Their Origin and Their Activity.* Clarendon.

PEKERIS, C. L., ACCAD, Y. & SHKOLLER, B. 1973 Kinematic dynamos and the earth's magnetic field. *Phil. Trans. R. Soc. Lond.* A **275**, 425–461.

PRESS, W. H., FLANNERY, B. P., TEUKOLSKY, S. A. & VETTERLING, W. T. 1989 *Numerical Recipes.* Cambridge University Press.

PROCTOR, M. R. E. 1977*a* On the eigenvalues of kinematic α-effect dynamos. *Astron. Nachr.* **298**, 19–25.

PROCTOR, M. R. E. 1977*b* The role of mean circulation in parity selection by planetary magnetic fields. *Geophys. Astrophys. Fluid Dyn.* **8**, 311–324.

ROBERTS, P. H. 1971 In *Dynamo theory of geomagnetism. World Magnetic Survey* (ed. A. J. Zmuda). *IAGA Bull.* **28**, pp. 123–132. International Union of Geodesy and Geophysics Publication Office.

ROBERTS, P. H. 1972 Kinematic dynamo models. *Phil. Trans. R. Soc. Lond.* A **271**, 663–697.

ROBERTS, P. H. 1987 Origin of the main field: dynamics. In *Geomagnetism*, Vol. 2 (ed. J. A. Jacobs). Academic Press.

ROBERTS, P. H. & GUBBINS, D. 1987 Origin of the main field: kinematics. In *Geomagnetism*, Vol. 2 (ed. J. A. Jacobs). Academic.

ROBERTS P. H. & STIX, M. 1971 *The Turbulent Dynamo: A Translation of a Series of Papers by F. Krause, K. H. Radler & M. Steenbeck.* Tech. Note 60. NCAR.

ROBERTS, P. H. & STIX, M. 1972 α-effect dynamos by the Bullard and Gellman formalism. *Astron. Astrophys.* **18**, 453–466.

SARSON, G. R. 1994 Kinematic dynamo calculations for geomagnetism. PhD thesis, University of Leeds.

SEREBRIANYA, P. M. 1988 Kinematic stationary geodynamo models with separated toroidal and poloidal motions. *Geophys. Astrophys. Fluid Dyn.* **44**, 141–164.

STEENBECK, M., KRAUSE, F. & RÄDLER, K.-H. 1966 A calculation of the mean electromotive force in an electrically conducting fluid in turbulent motion, under the influence of Coriolis forces. *Z. Naturforsch.* **21a**, 369–376. English translation in Roberts & Stix (1971).

WEISS, N. O. 1966 The expulsion of magnetic flux by eddies. *Proc. R. Soc. Lond.* A **293**, 310–328.

ZHANG, K. & BUSSE, F. H. 1987 On the onset of convection in rotating spherical shells. *Geophys. Astrophys. Fluid Dyn.* **39**, 119–147.

ZHANG, K. & BUSSE, F. H. 1989 Convection driven magnetohydrodynamic dynamos in rotating spherical shells. *Geophys. Astrophys. Fluid Dyn.* **49**, 97–116.